https://doi.org/10.5194/egusphere-2022-661
Preprint. Discussion started: 3 August 2022
© Author(s) 2022. CC BY 4.0 License.

From One-Dimensional to Three-Dimensional: Effect of Lateral Inhomogeneity on Tidal Gravity Derived by Analytical Expression

Zhenyu Wang[1]

[1]Institute of Earthquake Forecasting, China Earthquake Administration, Beijing 100036, China

Correspondence to: Zhenyu Wang (aayuyu11@163.com)

Abstract. Lateral inhomogeneity in Earth's mantle affects the tidal response. In this study, the analytical method for determining the effect of lateral inhomogeneity on tidal gravity, presented by Molodenskiy (1980), is introduced. Moreover, the current study reformulates the expressions for estimating the lateral inhomogeneity effects with respect to the unperturbed Earth and supplements some critical derivation process to enhance the method. The effects of lateral inhomogeneity are calculated using several real Earth models. By considering the collective contributions of seismic wave velocity disturbance and density disturbance, the global theoretical changes of semidiurnal gravimetric factor are obtained, which vary from −0.22% to 0.17% compared with those in a layered Earth model, no more than 1/3 of the ellipticity's effect. The gravity changes caused by laterally-inhomogeneous disturbance are also computed, and turn out to be up to 0.16% compared with the changes caused by tide-generating potential. The current study tests the importance of lateral inhomogeneity and other factors. The results indicate that the rotation, ellipticity, and inelasticity on tidal gravity are the most dominant factors, the ocean tide loading is the moderate one, and the lateral inhomogeneity is the least but not negligible factor, because the three-dimensional effect is comparable with ocean tide loading at some locations. Moreover, the amplitude of tidal gravity caused by lateral inhomogeneity is noticeable larger than the precision of superconducting gravimeters.

1 Introduction

Tides induced by gravitational attraction of the sun and moon constantly affect the shape and gravity field of Earth. The improvements in measurement techniques allow increasingly precise monitoring of periodic changes in geoid and gravity, which are concomitant with solid tides. The precision of the global positioning system (GNSS) and very long baseline interferometry (VLBI) in representing surface deformation is up to 1 mm (Petrov and Boy, 2004), and the iGrav superconducting gravimeter can detect gravity changes of 10^{-2} nm/s^2 (Rosat and Hinderer, 2018). These observations are of importance for investigating Earth's internal structures and dynamic processes (Yuan et al., 2013). Correspondingly, tidal theories have been developed to interpret and support the observations.

The first studies on tidal theory occurred in the early 20th century, with Love (1909) pioneering a method for calculating the tidal deformation of a spherically-stratified and non-rotating Earth. Longman (1963), Saito (1967), Farrell (1972), and

https://doi.org/10.5194/egusphere-2022-661
Preprint. Discussion started: 3 August 2022
© Author(s) 2022. CC BY 4.0 License.

Takeuchi and Saito (1972) gradually developed the tidal theory by taking account of spherical symmetry, elasticity, and isotropy of the Earth. Subsequently, Wahr (1981), Wahr and Bergen (1986), Dehant (1987), and de Vries and Wahr (1991) presented the expressions for computing the effects of rotation, inelastic mantle, solid inner core, and non-hydrostatic structure on the Earth's tide. Dehant et al. (1999) calculated tidal gravimetric factors for two rotating, non-spherical Earth models and determined that the results of an inelastic Earth model with a non-hydrostatic initial state are closer to measurements compared with those of an elastic Earth model in hydrostatic equilibrium. The majority of the aforementioned studies did not consider the direct effects of lateral inhomogeneity in the mantle. Although some studies taken account of mantle convection induced by lateral inhomogeneity, the treatments on rheology parameters remained one-dimensional.

In fact, the occurrence of plumes, volcanoes, large low shear velocity provinces, and other dynamic phenomena demonstrate that the interior of the Earth is far from homogeneous but full of large lateral variations. As a result, scientists have used the analytical or numerical methods to study solid tidal gravity in a three-dimensional Earth model. Métivier et al. (2006) used a spectral element method to develop a model of elastogravitational deformation which considers lateral inhomogeneity as well as non-hydrostatic pre-stress. Qin et al. (2014) proposed a semi-analytical method to compute solid tidal gravity for a laterally-heterogeneous Earth model. Lau et al. (2015) assembled a theoretical framework that permits the simulation of tidal deformation in an aspherical Earth model with an arbitrary equilibrium stress field. Tromp and Trampert (2018) demonstrated how effects of induced stress may be incorporated in seismic modelling and inversion. Lau and Faul (2019) developed and validated the method of Wahr and Bergen (1986) using measurements and calculated the effects of inelasticity on tidal gravity. All of the aforementioned, indeed, most of the recent tidal studies are based on the work of the classical Dahlen and Tromp (2021) book (Theoretical Global Seismology). These studies are mainly based on numerical approaches. The numerical approaches have many advantages, e.g., considering the effects of mantle convection and plate movements, over analytical approaches. On the other hand, analytical approaches are more flexible when combining with seismology and gravity models. As a result, it is worthy introducing and developing the analytical approach for calculating the effect of inhomogeneity on deformation issues.

The first efforts of analytical approach started from 1980s by Molodenskiy. Although Molodenskiy (1977, 1980) presented analytical expressions for determining changes to the tidal gravimetric factor induced by lateral inhomogeneity, only the effects of seismic waves have been considered. Molodenskii and Kramer (1980) based on the work of Molodenskiy (1980) to evaluate the changes in gravimetric factor for a simple laterally-heterogeneous ocean-land model. After that, Wang (1991, 1994, 1997) developed the three-dimensional tidal theory more comprehensively and systematically, considering the contributions of rotation, spherical asymmetry, visco-elasticity, and lateral inhomogeneity, and discussed the effect of non-hydrostatic pre-stress, which greatly improved the three-dimensional tidal theory in the field of analytical solution. Fu and Sun (2007) developed the tidal theory by determining the effects of laterally varying densities in the mantle on tidal gravity, and showed that the effects are comparable with those of laterally-varying seismic wave velocities.

The aim of this study is to present formulae for representing the effects of laterally-inhomogeneity in the mantle on tidal gravimetric factors with a new analytical approach (presented by Molodenskiy, 1977, but new for most readers) and to

https://doi.org/10.5194/egusphere-2022-661
Preprint. Discussion started: 3 August 2022
© Author(s) 2022. CC BY 4.0 License.

determine whether the effects are comparable with other factors, e.g., rotation, ellipticity, and ocean tide loading. Firstly, the analytical expressions for computing the effects of laterally-inhomogeneity on tidal gravimetric factors are presented. Then the effects of lateral inhomogeneity on gravimetric factors and gravity are computed using various three-dimensional Earth models. Finally, the tidal gravity changes caused by laterally-inhomogeneous disturbance are calculated and compared with those caused by tide-generating potential, rotation and ellipticity, and ocean tide loading.

2 Basic Tidal Theory for a One-Dimensional Earth Model

The tidal theory presented in the current study starts from a system of equations describing an elastic, self-gravitational, and spherically-symmetrical Earth model. The equilibrium, constitutive, and Poisson equations (Farrell, 1972; Takeuchi and Saito, 1972) are:

$$L(\boldsymbol{u},\Psi) = \rho g \boldsymbol{e}_r(\nabla\cdot\boldsymbol{u}) + \rho\nabla(\Psi - g u_r) + \nabla\cdot\tau = 0 \tag{1}$$

$$\tau = \lambda \mathbf{I}\nabla\cdot\boldsymbol{u} + \mu(\nabla\boldsymbol{u} + (\nabla\boldsymbol{u})^T) \tag{2}$$

$$\nabla^2\Psi = -4\pi G(\delta\rho) = 4\pi G\nabla\cdot(\rho\boldsymbol{u}) \tag{3}$$

In Equations (1) - (3), $\boldsymbol{u}$ is the displacement vector, Ψ is the gravitational potential changes, ρ is density, g is gravity, $\boldsymbol{e}$ is unit vector, subscript r indicates the radial direction, τ is stress tensor, or incremental stress with respect to initial static stress (Dahlen, 1972; Wang, 1991), λ and μ are Lame's constants, and G is Newton's gravitational constant. Equations (1) - (3) are reduced to dimensionless form for convenience. The values of the rheology parameter λ_0, density ρ_0 at the center and gravity g_0 on the surface of the Earth are denoted as the unit rheology parameter, unit density, and unit gravity, respectively. Displacement $\boldsymbol{u}$, stress tensor component $\tau\cdot\boldsymbol{e}_r$, and potential changes Ψ during tidal deformation can be expanded into a series of spherical harmonic functions:

$$\boldsymbol{u}^0 = \sum_{n_0=0}^{\infty}\sum_{m_0=-n_0}^{n_0}\boldsymbol{u}^{n_0m_0} = \sum_{n_0=0}^{\infty}\sum_{m_0=-n_0}^{n_0}\left[y_1(r;n,m)\boldsymbol{R}_{n_0}^{m_0}(\theta,\phi) + y_3(r;n,m)\boldsymbol{S}_{n_0}^{m_0}(\theta,\phi)\right] \tag{4}$$

$$\tau^0\cdot\boldsymbol{e}_r = \sum_{n_0=0}^{\infty}\sum_{m_0=-n_0}^{n_0}\boldsymbol{T}^{n_0m_0} = \sum_{n_0=0}^{\infty}\sum_{m_0=-n_0}^{n_0}\left[y_2(r;n,m)\boldsymbol{R}_{n_0}^{m_0}(\theta,\phi) + y_4(r;n,m)\boldsymbol{S}_{n_0}^{m_0}(\theta,\phi)\right] \tag{5}$$

$$\Psi^0 = \sum_{n_0=0}^{\infty}\sum_{m_0=-n_0}^{n_0}\Psi^{n_0m_0} = \sum_{n_0=0}^{\infty}\sum_{m_0=-n_0}^{n_0}y_5(r;n,m)Y_{n_0}^{m_0}(\theta,\phi) \tag{6}$$

The subscript and superscript 0 indicate variables of the spherically-symmetrical model, distinct from those of the spherically-asymmetrical model (see below). The Toroidal component of the model is not considered as Fu and Sun (2007) have confirmed that this component makes no contribution to changes in gravity. In Equations (4) - (6),

$$\boldsymbol{R}_{n_0}^{m_0}(\theta,\phi) = \boldsymbol{e}_r Y_{n_0}^{m_0}(\theta,\phi) \tag{7}$$

$$\boldsymbol{S}_{n_0}^{m_0}(\theta,\phi) = \left[\boldsymbol{e}_\theta\frac{\partial}{\partial\theta} + \boldsymbol{e}_\phi\frac{1}{\sin\theta}\frac{\partial}{\partial\phi}\right]Y_{n_0}^{m_0}(\theta,\phi) \tag{8}$$

https://doi.org/10.5194/egusphere-2022-661
Preprint. Discussion started: 3 August 2022
© Author(s) 2022. CC BY 4.0 License.

$$Y_{n_0}^{m_0}(\theta,\phi) = P_{n_0}^{m_0}(\cos\theta)\begin{cases}\cos m_0\phi \\ \sin m_0\phi\end{cases} \tag{9}$$

In Equations (7) - (9), $\boldsymbol{e}_r$, $\boldsymbol{e}_\theta$, and $\boldsymbol{e}_\phi$ are unit vectors, $P_{n_0}^{m_0}(\cos\theta)$ is the Legendre function for degree n_0 and order m_0. The use of sine or cosine in Equation (9) is determined in Section 5. $y_6(r)$ is defined as follows according to Longman (1963):

$$y_6(r;n,m) = \dot{y}_5(r;n,m) - 4\pi G\rho y_1(r;n,m) \tag{10}$$

In Equation (10), the dot indicates a derivative with regard to r, coefficients $y_i(r;n,m), i = 1,\dots,6$ for specific problems (not confined to tide) can be determined using the boundary conditions by substituting Equations (4) - (6) and (10) into Equations (1) - (3), as shown in Appendix A.

Gravity variations $\Delta g(r,\theta,\phi)$ consist of the radial derivative of potential changes Ψ and the contribution of displacement. On the free surface:

$$\Delta g(a,\theta,\phi) = -\frac{\partial\Psi}{\partial r}\Big|_a - \beta u_r(a,\theta,\phi) \tag{11}$$

In Equation (11), β denotes the free-air gravity gradient, a is the surface radius, and $u_r(a,\theta,\phi)$ is the radial displacement. According to Sun and Okubo (1993):

$$-\frac{\partial\Psi}{\partial r}\Big|_a = \frac{g_0 UdS}{a^3}\sum_{n=0}^{\infty}\sum_{m=-n}^{n}[(n+1)y_5(a;n,m)]Y_n^m(\theta,\phi) \tag{12}$$

g_0 denotes the gravity on the Earth's surface, U denotes the unit displacement or dislocation, and dS denotes an infinitesimal surface. Although Equation (12) is proposed for dislocation issues, it's suitable for tidal issues as well since the numerator is normalized later. Equation (11) may be rewritten as:

$$\Delta g(a,\theta,\phi) = \frac{g_0 UdS}{a^3}\sum_{n=0}^{\infty}\sum_{m=-n}^{n}[(n+1)y_5(a;n,m)]Y_n^m(\theta,\phi) - \frac{\beta UdS}{a^2}\sum_{n=0}^{\infty}\sum_{m=-n}^{n}[y_1(a;n,m)]Y_n^m(\theta,\phi) \tag{13}$$

for $\beta = \frac{2g_0}{a}$, Equation (13) becomes:

$$\Delta g(a,\theta,\phi) = \frac{g_0 UdS}{a^3}\sum_{n=0}^{\infty}\sum_{m=-n}^{n}[(n+1)y_5(a;n,m)]Y_n^m(\theta,\phi) - \frac{2g_0 UdS}{a^3}\sum_{n=0}^{\infty}\sum_{m=-n}^{n}[y_1(a;n,m)]Y_n^m(\theta,\phi) \tag{14}$$

Using the unit of $g_0 UdS = 1$ and $a = 1$, Equation (14) is simplified as:

$$\Delta g(a,\theta,\phi) = \sum_{n=0}^{\infty}\sum_{m=-n}^{n}[(n+1)y_5(1;n,m) - 2y_1(1;n,m)]Y_n^m(\theta,\phi) \tag{15}$$

Equation (15) shows that variations in gravity resulting from the tide can be computed by coefficients y_1 and y_5.

3 Tidal Theory for a Three-Dimensional Earth Model

Since the Earth is in reality not spherically-symmetrical, the effects of lateral inhomogeneity must be considered. The most significant effect is that adding the asymmetric increments $\delta\lambda(r,\theta,\phi)$, $\delta\mu(r,\theta,\phi)$, and $\delta\rho(r,\theta,\phi)$ to the spherically-

https://doi.org/10.5194/egusphere-2022-661
Preprint. Discussion started: 3 August 2022
© Author(s) 2022. CC BY 4.0 License.

symmetrical model increases the difficulty in expanding $\boldsymbol{u}$ and Ψ. Consequently, the variations in gravity cannot be directly computed. Molodenskiy (1977) resolved this problem based on the perturbation method by separating the effects of asymmetrical increments from those of the spherically-symmetrical model, and presented analytical expressions for computing the effects of asymmetrical increments on tidal gravity using auxiliary solutions. According to this method:

$$\boldsymbol{u} = \boldsymbol{u}^0 + \delta\boldsymbol{u} \tag{16}$$

$$\Psi = \Psi^0 + \delta\Psi \tag{17}$$

In Equations (16) and (17), $\boldsymbol{u}^0$ and Ψ^0 are the unperturbed solutions for the spherically-symmetrical model, $\delta\boldsymbol{u}$ and $\delta\Psi$ are the perturbed solutions for asymmetrical increments.

Similar to Equations (4) and (6):

$$\delta\boldsymbol{u} = \sum_{n=0}^{\infty}\sum_{m=-n}^{n}\delta\boldsymbol{u}^{nm} = \sum_{n=0}^{\infty}\sum_{m=-n}^{n}[y_1^*(r;n,m)\boldsymbol{R}_n^m(\theta,\phi) + y_3^*(r;n,m)\boldsymbol{S}_n^m(\theta,\phi)] \tag{18}$$

$$\delta\Psi = \sum_{n=0}^{\infty}\sum_{m=-n}^{n}\delta\Psi^{nm} = \sum_{n=0}^{\infty}\sum_{m=-n}^{n}y_5^*(r;n,m)Y_n^m(\theta,\phi) \tag{19}$$

In Equations (18) and (19), $y_i^*(r;n,m)$ are the expanded coefficients of perturbed solutions. The effects of lateral inhomogeneity on gravity can be obtained once the coefficients are determined and substituted into Equation (15). In contrast to the coefficients of unperturbed solutions, those of perturbed solutions cannot be directly computed using the method shown in Appendix A, since the boundary conditions of the coefficients are uncertain. In classical approach, researchers solved this problem by establishing differential equations (Lau and Faul, 2019; Lau et al., 2015; Métivier et al., 2006, 2007). Molodenskiy (1977) proposed an analytical method to determine the coefficients basing on the Betti Reciprocal theorem, assuming that the effects of lateral inhomogeneity can be replaced by simple external forces on an unperturbed Earth. Consequently, the boundary conditions become determinable. By reformulating and perturbating Equations (1) and (3):

$$L_i(\delta\boldsymbol{u},\delta\Psi) + \delta L_i(\boldsymbol{u}^0,\Psi^0) = 0 \tag{20}$$

$$\Delta(\delta\Psi) = 4\pi G\nabla\cdot(\delta\rho\boldsymbol{u} + \rho\delta\boldsymbol{u}) \tag{21}$$

In Equations (20) and (21), the subscripts $i = 1,2,3$ are the three components of the coordinate system. Here, the auxiliary solutions $\boldsymbol{u}_i^j$ and $\Psi^j, j = 1,2,3$ are defined, which are displacement and potential changes of the unperturbed Earth resulting from external forces, respectively. These auxiliary solutions have no physical significance, although their forms are similar to those of pressure ($j = 1$), shear ($j = 2$), and tidal attraction ($j = 3$), since they are purely defined to determine the perturbed solutions. The auxiliary solutions satisfy the following equations:

$$L_i(\boldsymbol{u}^j,\Psi^j) = 0 \tag{22}$$

$$\Delta\Psi^j = 4\pi G\nabla\cdot(\rho\boldsymbol{u}^j) \tag{23}$$

By multiplying Equations (20) and (22) by u_i^j and $-\delta u_i$, the results over three directions of $i = 1,2,3$ are summarized, and by integrating the result over the volume:

https://doi.org/10.5194/egusphere-2022-661
Preprint. Discussion started: 3 August 2022
© Author(s) 2022. CC BY 4.0 License.

$$\iiint u_i^j \, \delta L_i(\boldsymbol{u}^0, \Psi^0) dv + I = 0 \tag{24}$$

Therein:

$$\delta L_i(\boldsymbol{u}^0, \Psi^0) = \delta\rho\{-\nabla_i V(\nabla \cdot \boldsymbol{u}^0) + \nabla_i[\Psi^0 + (\boldsymbol{u}^0, \nabla V)]\} + \rho[-\nabla_i \delta V(\nabla \cdot \boldsymbol{u}^0) + \nabla_i(\boldsymbol{u}^0, \nabla \delta V)] + \nabla_k \delta\tau_{ik} \tag{25}$$

$$I = \iiint \left[u_i^j L_i(\delta\boldsymbol{u}, \delta\Psi) - \delta u_i L_i(\boldsymbol{u}^j, \Psi^j)\right] dv \tag{26}$$

In Equations (25) and (26), V is the gravitational potential, δV is the disturbance of potential resulting from $\delta\rho$, $\delta\tau_{ik}$ denotes disturbance of stress tensor. In Equation (25), $(\boldsymbol{u}^0, \nabla V)$ is the inner product. Note that $g\boldsymbol{e}_r$ (Equation 1) is replaced with $\nabla_i V$ for the reason that the Earth model is no more spherically symmetric, thus the gravity is no more radially oriented. With mathematical work (see details in Appendix B), Equation (26) becomes:

$$I = \frac{4\pi(n+m)!}{\varepsilon_m(2n+1)(n-m)!} \cdot \left\{-y_1^*(1;n,m)y_2^j(1) - n(n+1)y_3^*(1;n,m)y_4^j(1) - \frac{1}{4\pi G} y_5^*(1;n,m)\left[y_6^j(1) + (n+1)y_5^1(1)\right]\right\}$$
$$- \iiint \Psi^j \nabla \cdot (\delta\rho \boldsymbol{u}^0)\, dv + \iint \left(u_i^j \delta\tau_{ik} + \Psi^j u_k^0 \delta\rho\right) dS_k \tag{27}$$

therein:

$$\varepsilon_m = \begin{cases} 1 & m = 0 \\ 2 & m \neq 0 \end{cases}$$

$$\delta\tau_{ik}|_S = -\left[\delta\mu\left(\frac{\partial u_i^0}{\partial x_k} + \frac{\partial u_k^0}{\partial x_i}\right) + \delta\lambda \nabla \cdot (\boldsymbol{u}^0)\delta_{ik}\right]\Bigg|_S$$

$$dS_k = \frac{x_k}{r} dS$$

According to the divergence theorem, the last term on the right-hand side of Equation (27) becomes:

$$\iint \left(u_i^j \delta\tau_{ik} + \Psi^j u_k^0 \delta\rho\right) dS_k = \iiint \nabla_k \cdot \left(u_i^j \delta\tau_{ik} + \Psi^j u_k^0 \delta\rho\right) dv$$
$$= \iiint \left\{-\frac{\partial u_i^j}{\partial x_k}\left[\delta\mu\left(\frac{\partial u_i^0}{\partial x_k} + \frac{\partial u_k^0}{\partial x_i}\right) + \delta\lambda \nabla \cdot (\boldsymbol{u}^0)\delta_{ik}\right] - u_i^j \nabla_k \delta\tau_{ik} + \Psi^j \nabla \cdot (\delta\rho \boldsymbol{u}^0) + \delta\rho(\boldsymbol{u}^0, \nabla\Psi^j)\right\} dv \tag{28}$$

By substituting Equations (25), (27), and (28) into Equation (24) through simple manipulations:

$$F^j(\delta\rho, \delta\mu, \delta\lambda) = \frac{4\pi(n+m)!}{\varepsilon_m(2n+1)(n-m)!}$$
$$\cdot \left[y_1^*(1;n,m)y_2^j(1) + n(n+1)y_3^*(1;n,m)y_4^j(1) + \frac{1}{4\pi G} y_5^*(1;n,m)\left[y_6^j(1) + (n+1)y_5^1(1)\right]\right] \tag{29}$$

where:

$$F^j(\delta\rho, \delta\mu, \delta\lambda) = \iiint \left[\overbrace{\delta\rho(\boldsymbol{u}^0, \nabla\Psi^j) + u_i^j \delta L_{i\rho}(\boldsymbol{u}^0, \Psi^0)}^{\delta\rho} \overbrace{-\delta\mu\left(\frac{\partial u_i^0}{\partial x_k} + \frac{\partial u_k^0}{\partial x_i}\right)\frac{\partial u_i^j}{\partial x_k}}^{\delta\mu} \underbrace{-\delta\lambda \nabla \cdot (\boldsymbol{u}^0)\nabla \cdot (\boldsymbol{u}^j)}_{\delta\lambda}\right] dv \tag{30}$$

$$\delta L_{i\rho}(\boldsymbol{u}^0, \Psi^0) = \delta\rho\{-\nabla_i V(\nabla \cdot \boldsymbol{u}^0) + \nabla_i[\Psi^0 + (\boldsymbol{u}^0, \nabla V)]\} + \rho[-\nabla_i \delta V(\nabla \cdot \boldsymbol{u}^0) + \nabla_i(\boldsymbol{u}^0, \nabla \delta V)] \tag{31}$$

https://doi.org/10.5194/egusphere-2022-661
Preprint. Discussion started: 3 August 2022
© Author(s) 2022. CC BY 4.0 License.

In Equation (30), the first two terms on the right-hand side are related to $\delta\rho$ (Fu and Sun, 2007; Wang, 1991). The third and fourth term are related to $\delta\mu$ and $\delta\lambda$, respectively (Molodenskiy, 1980).

According to Equation (29), the following expressions can be considered as boundary conditions for auxiliary solutions to calculate the perturbed solutions $y_i^*(1;n,m)$.

$$\begin{aligned} &1)\ j=1 \quad y_2^1(1)=1 \qquad y_4^1(1)=0 \qquad y_6^1(1)+(n+1)y_5^1(1)=0 \\ &2)\ j=2 \quad y_2^2(1)=0 \quad y_4^2(1)=\frac{1}{n(n+1)} \quad y_6^1(1)+(n+1)y_5^1(1)=0 \\ &3)\ j=3 \quad y_2^3(1)=0 \qquad y_4^3(1)=0 \qquad y_6^1(1)+(n+1)y_5^1(1)=4\pi G \end{aligned} \tag{32}$$

Note that the above boundary conditions are different from Fu and Sun (2007) because the definitions of y_6 are not the same. Both unperturbed solutions and auxiliary solutions are determined by integrating the differential equations by Runge-Kutta method. The specific treatments on external core and integrating method have been presented by Longman (1963) and Wang et al. (2012).

The following can be derived:

$$F^j(\delta\rho,\delta\mu,\delta\lambda)=c(n,m)\begin{cases} y_1^*(1;n,m), & j=1 \\ y_3^*(1;n,m), & j=2 \\ y_5^*(1;n,m), & j=3 \end{cases} \tag{33}$$

$$c(n,m)=\iint \left(Y_n^m(\theta,\phi)\right)^2 dS=\frac{4\pi(n+m)!}{\varepsilon_m(2n+1)(n-m)!} \tag{34}$$

The boundary conditions shown in Equation (32) are similar to those of pressure, shear, and tide problems, respectively. But actually auxiliary solutions have no physical significance. For the right-hand side of Equation (33), only $y_1^*(1;n,m)$ and $y_5^*(1;n,m)$ affect gravity. Once these two terms are determined and substituted into Equation (15), the effects of lateral inhomogeneity on surface gravity can be obtained. It should be noted that the special cases of $n=0$ and $n=1$ require further treatment, with a more detailed description in relative studies (Fu and Sun, 2007; Wang, 1991).

4 Expressions of the Quadrature $F^j(\delta\rho,\delta\mu,\delta\lambda)$

As mentioned above, obtaining the quadrature $F^j(\delta\rho,\delta\mu,\delta\lambda)$ is crucial to determine $y_i^*(1;n,m)$. $F^j(\delta\rho,\delta\mu,\delta\lambda)$ can be decomposed into three parts as:

$$F^j(\delta\rho,\delta\mu,\delta\lambda)=F^j(\delta\rho)+F^j(\delta\mu)+F^j(\delta\lambda) \tag{35}$$

In Equation (35), $F^j(\delta\rho)$, $F^j(\delta\mu)$, and $F^j(\delta\lambda)$ correspond to the effects of $\delta\rho$, $\delta\mu$, and $\delta\lambda$, respectively. These terms on the right-hand side of Equation (35) have been meticulously defined by Fu and Sun (2007), Molodenskiy (1980), and Wang (1991). The present study addresses the expressions for the three terms on the right-hand side directly as below:

$$F_{nm}^j(\delta\lambda)=-\sum_{l=0}^{N_e}\sum_{p=-l}^{l}A_{lpnmn_0m_0}\int_0^1\lambda_{lp}(r)x_{nn_0}^{(1)(j)}(r)dr \tag{36}$$

https://doi.org/10.5194/egusphere-2022-661
Preprint. Discussion started: 3 August 2022
© Author(s) 2022. CC BY 4.0 License.

$$F_{nm}^{j}(\delta\mu) = -\sum_{l=0}^{N_e}\sum_{p=-l}^{l} A_{lpnmn_0m_0}\int_0^1 r^{n+n_0}\mu_{lp}(r)\left[x_{nn_0}^{(2)(j)}(r) + nn_0 x_{nn_0}^{(3)(j)}(r) + nn_0(nn_0 - n_0 - n + 3)x_{nn_0}^{(4)(j)}(r)\right]dr \quad (37)$$

$$F_{nm}^{j}(\delta\rho) = -\sum_{l=0}^{N_e}\sum_{p=-l}^{l} A_{lpnmn_0m_0}\int_0^1 \rho(r)\left\{\gamma_{lp}^{1}(r)\left[x_{nn_0}^{(5)(j)}(r) + nn_0 x_{nn_0}^{(6)(j)}(r)\right]\right.$$
$$\left. + \gamma_{lp}^{2}(r)\left[x_{nn_0}^{(7)(j)}(r) - l x_{nn_0}^{(8)(j)}(r) + nn_0 x_{nn_0}^{(9)(j)}(r) + l n x_{nn_0}^{(10)(j)}(r)\right] + \gamma_{lp}^{3}(r)x_{nn_0}^{(11)(j)}(r)\right\}dr \quad (38)$$

$$A_{lpnmn_0m_0} = \iint Y_l^p(\theta,\phi)Y_n^m(\theta,\phi)Y_{n_0}^{m_0}(\theta,\phi)dS \quad (39)$$

$$\begin{cases}\gamma^1 = \delta\rho/\rho \\ \gamma^2 = \delta g/g \\ \gamma^3 = \delta\dot{g}/\dot{g}\end{cases} \quad (40)$$

In Equations (36) - (38), $\lambda_{lp}(r)$, $\mu_{lp}(r)$, $\gamma_{lp}^1(r)$, $\gamma_{lp}^2(r)$, and $\gamma_{lp}^3(r)$ are spherical harmonic expansion coefficients for $\delta\lambda$, $\delta\mu$, $\delta\rho/\rho$, $\delta g/g$, and $\delta\dot{g}/\dot{g}$, respectively, N_e is the convergent degree of the three-dimensional Earth model, n and m are the expansion degree and order for auxiliary solutions, respectively, and n_0 and m_0 are the degree and order for the tidal component of interest, respectively. The treatment of $A_{lpnmn_0m_0}$ is shown in Appendix C and definitions of coefficients $x_{nn_0}^{(i)(j)}(r)$ can be found in Appendix D.

Note that Equations (36) - (38) do not contain the effect of non-hydrostatic pre-stress, which arises from transition from a one-dimensional Earth model to a three-dimensional one. The majority of previous studies considered the effects of non-hydrostatic pre-stress to be negligible. Molodenskii and Kramer (1980) and Vermeersen and Vlaar (1991) concluded that the effects of non-hydrostatic pre-stress resulting from density disturbance together with the effects of density disturbance can be neglected since they considered the density disturbance to be much smaller than seismic wave velocity disturbance. Since Geller (1988) and Fu and Sun (2007) assumed that the time scales of tidal deformation are much lower than those of dynamic processes, they considered the Earth to be in a quasi-equilibrium state and that incremental stress is negligible. Besides, other results suggest that the effect of non-hydrostatic pre-stress on gravity can be neglected. Wang (1991) calculated the perturbation of generalized hydrostatic pressure and considered that it should represent the main contribution of non-hydrostatic pre-stress, and the effect is not comparable with those of rotation or ellipticity. Métivier et al. (2007) computed the effects of non-hydrostatic pre-stress based on the spectral element method and argued that the effects can be neglected. Consequently, basing on the above discussion and the fact that non-hydrostatic pre-stress effect cannot be determined uniquely by density perturbation for the existence of dynamic topography and plate movement, the non-hydrostatic pre-stress is not included in this paper.

https://doi.org/10.5194/egusphere-2022-661
Preprint. Discussion started: 3 August 2022
© Author(s) 2022. CC BY 4.0 License.

5 Final Formulae for Tidal Gravimetric Factors in a Three-Dimensional Inhomogeneous Earth Model

Since the expressions for $F^j(\delta\rho, \delta\mu, \delta\lambda)$ are determined, the final formulae for the effects of lateral inhomogeneity on gravity can be obtained using Equations (15) and (33). These effects can be regarded as gravity changes Δg resulting from lateral inhomogeneity respective to the layered Earth. In purpose of decomposing the effects as shown in Equation (35), elastic parameters $\delta\lambda$ and $\delta\mu$ are linked with seismic wave velocities α and β and density γ^1 through a linear relation that assumes a kind of thermal relationship (Fu and Sun, 2007):

$$\delta\lambda = 2(\lambda + 2\mu)\alpha - 4\mu\beta + \lambda\gamma^1 \tag{41}$$

$$\delta\mu = 2\mu\beta + \mu\gamma^1 \tag{42}$$

In above equations, $\alpha = \delta v_p / v_p$, $\beta = \delta v_s / v_s$, and $\gamma^1 = \delta\rho/\rho$. δv_p, δv_s, and $\delta\rho$ are the spherically-asymmetrical increments for P-wave velocity, S-wave velocity, and density, respectively. v_p, v_s, and ρ are mean values of the angle variables with regard to r for P-wave velocity, S-wave velocity, and density, respectively. As shown in Appendix E, with some manipulations, the following is obtained:

$$\begin{aligned}\Delta g(\theta,\phi) = \sum_{l=0}^{N_e}\sum_{p=-l}^{l}\{&\left[\Delta g_{p1}(\theta,\phi) + \Delta g_{s1}(\theta,\phi) + \Delta g_{\rho 1}(\theta,\phi)\right]\cos m_0\phi \\ &+ \left[\Delta g_{p2}(\theta,\phi) + \Delta g_{s2}(\theta,\phi) + \Delta g_{\rho 2}(\theta,\phi)\right]\sin m_0\phi\}\end{aligned} \tag{43}$$

where,

$$\Delta g_{p1}(\theta,\phi) = \sum_{n=|l-n_0|}^{l+n_0} \frac{E_{lpn(p\pm m_0)n_0m_0}}{c(n,p\pm m_0)} I(p,p\pm m_0,m_0) Y_n^{p\pm m_0}(\theta,\phi) \int_b^1 2(\lambda+2\mu) y_n(r)\alpha_{lp}(r)dr \tag{44}$$

$$\Delta g_{s1}(\theta,\phi) = \sum_{n=|l-n_0|}^{l+n_0} \frac{E_{lpn(p\pm m_0)n_0m_0}}{c(n,p\pm m_0)} I(p,p\pm m_0,m_0) Y_n^{p\pm m_0}(\theta,\phi) \int_b^1 \{2\mu[z_n(r) - 2y_n(r)]\beta_{lp}(r)\}dr \tag{45}$$

$$\begin{aligned}\Delta g_{\rho 1}(\theta,\phi) = \sum_{n=|l-n_0|}^{l+n_0} &\frac{E_{lpn(p\pm m_0)n_0m_0}}{c(n,p\pm m_0)} I(p,p \\ &\pm m_0,m_0) Y_n^{p\pm m_0}(\theta,\phi) \int_b^1 \rho(r)\{[q_n^1(r) + \lambda y_n(r) + \mu z_n(r)]\gamma_{lp}^1(r) + q_n^2(r)\gamma_{lp}^2(r) + q_n^3(r)\gamma_{lp}^3(r)\}dr\end{aligned} \tag{46}$$

In Equation (44), $\Delta g_{p1}(\theta,\phi)$ is the summation of $\Delta g_{p1}^+(\theta,\phi)$ and $\Delta g_{p1}^-(\theta,\phi)$, which correspond to replacing "±" with "+" and "−", respectively. The same treatment is also applied to Equations (45) and (46). The expressions of $y_n(r)$, $z_n(r)$, and $q_n^i(r), i = 1, \ldots, 7$ are shown in Appendix E.

As a variational approach is used to transfer volumetric integrals of elastogravitational equations towards simple surface integrals (Equations 20, 21, and Appendix B), which means that the Lame's parameters and density are assumed to be continuous within the volume. Yet within the Earth which composes of various interfaces, the parameters are usually

https://doi.org/10.5194/egusphere-2022-661
Preprint. Discussion started: 3 August 2022
© Author(s) 2022. CC BY 4.0 License.

discontinuous. To handle this issue, Equations (44) - (46) are integrated layer by layer. Besides, the core-mantle boundary is dealt with the approach of Longman (1963).

In Equations (44) - (46):

$$I(p, p \pm m, m_0) = \int_0^{2\pi} \cos m_0\phi \begin{Bmatrix} \cos p\phi \\ \sin p\phi \end{Bmatrix} \begin{Bmatrix} \cos(p \pm m_0)\phi \\ \sin(p \pm m_0)\phi \end{Bmatrix} d\phi \tag{47}$$

$$Y_n^{p\pm m_0}(\theta, \phi) = P_n^{p\pm m_0}(\cos\theta) \begin{Bmatrix} \cos(p \pm m_0)\phi \\ \sin(p \pm m_0)\phi \end{Bmatrix} \tag{48}$$

The expressions of $\Delta g_{p2}(\theta, \phi)$, $\Delta g_{s2}(\theta, \phi)$, and $\Delta g_{\rho 2}(\theta, \phi)$ are the same as those of $\Delta g_{p1}(\theta, \phi)$, $\Delta g_{s1}(\theta, \phi)$, and $\Delta g_{\rho 1}(\theta, \phi)$, with the only difference being the replacement of $\cos m_0\phi$ in Equation (47) with $\sin m_0\phi$. The use of the sine and cosine in the last two terms of Equations (47) and (48) is determined as follows:

(1) The second factor in Equation (47) is $\cos p\phi$ when $\alpha_{lp}(r)$, $\beta_{lp}(r)$, and $\gamma_{lp}^1(r)$ are the coefficients of $\cos p\phi$, whereas the second factor is $\sin p\phi$ when $\alpha_{lp}(r)$, $\beta_{lp}(r)$, and $\gamma_{lp}^1(r)$ are the coefficients of $\sin p\phi$;

(2) The third factor in Equation (47) is $\cos(p \pm m_0)\phi$ when the first two factors in Equation (47) are both sines or both cosines, otherwise the third factor is $\sin(p \pm m_0)\phi$;

(3) When the third factor in Equation (47) is $\cos(p \pm m_0)\phi$, Equation (48) is written as:

$$Y_n^{p\pm m_0}(\theta, \phi) = P_n^{p\pm m_0}(\cos\theta)\cos(p \pm m_0)\phi$$

When the third factor in Equation (47) is $\sin(p \pm m_0)\phi$, Equation (48) is written as:

$$Y_n^{p\pm m_0}(\theta, \phi) = P_n^{p\pm m_0}(\cos\theta)\sin(p \pm m_0)\phi$$

Finally, the changes of gravimetric factor δ_1 and phase Φ_1 are obtained:

$$\delta_1(\theta, \phi) = \frac{1}{\delta_{n_0} P_{n_0}^{m_0}(\cos\theta)} \sum_{l=0}^{N_e} \sum_{p=-l}^{l} \{\Delta g_1(\theta, \phi)\cos m_0\phi + \Delta g_2(\theta, \phi)\sin m_0\phi\}$$

$$\Phi_1(\theta, \phi) = \frac{1}{\delta_{n_0} P_{n_0}^{m_0}(\cos\theta)} \sum_{l=0}^{N_e} \sum_{p=-l}^{l} \{\Delta g_2(\theta, \phi)\cos m_0\phi - \Delta g_1(\theta, \phi)\sin m_0\phi\} \tag{49}$$

In Equation (49), $\Delta g_1(\theta, \phi)$ is the summation of $\Delta g_{p1}(\theta, \phi)$, $\Delta g_{s1}(\theta, \phi)$, and $\Delta g_{\rho 1}(\theta, \phi)$. $\Delta g_2(\theta, \phi)$ is the summation of $\Delta g_{p2}(\theta, \phi)$, $\Delta g_{s2}(\theta, \phi)$, and $\Delta g_{\rho 2}(\theta, \phi)$. The gravimetric factor is written as:

$$\delta_{n_0} = 1 - \frac{n_0 + 1}{n_0} k_{n_0} + \frac{2}{n_0} h_{n_0} \tag{50}$$

In Equation (50), h_{n_0} and k_{n_0} are tidal Love numbers of degree n_0, describing the variations in vertical displacement and gravitational potential at the surface, respectively.

https://doi.org/10.5194/egusphere-2022-661
Preprint. Discussion started: 3 August 2022
© Author(s) 2022. CC BY 4.0 License.

6 Numerical Results: Effects of Lateral Inhomogeneity

6.1 Global Distribution of the Theoretical Semidiurnal Tidal Gravimetric Factor

With the above sections have introduced the analytical solution for determining the effects of lateral inhomogeneity, this section display the numerical results. The current study adopts the three-dimensional Earth model GyPSuM (Simmons et al., 2010) to determine the effects of lateral inhomogeneity. The model is developed through simultaneous inversion of seismic wave travel times and geodynamic observations. GyPSuM incorporates models of P-wave velocity, S-wave velocity, and density, which can be downloaded from the Incorporated Research Institutions for Seismology (IRIS) website (http://ds.iris.edu/ds/products/emc-Earthmodels/, Trabant et al., 2012). As mentioned above, the current study also requires the three-dimensional gravity model and its derivatives for computing. The approaches to obtain gravity model vary between different researches. In this study, in light of that the contribution of gravity model is much smaller than those of the seismic wave velocity model and density model (Fu and Sun, 2007), the gravity model is determined by directly integrating the density model.

Once the Earth model is identified, the effects of lateral inhomogeneity on semidiurnal gravimetric factors can be computed with the use of Equation (49). It should be noted that the polar effects are observable in the results, e.g., the values in the north and south poles are dramatically larger than other regions. Because the denominator approaches 0 with an increase in latitude, the numerical error at polar regions may be amplified. This error has little influence on middle-low latitude regions which is the focus of the current study and is hard to avoid. Therefore, the current study shows the results from 75°S to 75°N only.

Fig. 1 shows the changes in the semidiurnal gravimetric factors calculated using the GyPSuM P-wave model, S-wave model, and density model, which range from −0.24% to 0.32%, −0.33% to 0.21%, and −0.12% to 0.09%, respectively. Fig. 1a and 1b show similar patterns with generally opposite signs, and this feature is also evident in the results for the previous studies (Fu and Sun, 2007; Molodenskii and Kramer, 1980; Wang, 1991). The effects of P-wave velocity disturbance are generally positive (negative) under continents (oceans), whereas S-wave velocity disturbance has the opposite effects. Although the patterns of density disturbance effects are similar with those of S-wave velocity disturbance, the magnitude of the former is notably smaller than the later, with a factor of about 0.3. Generally, the gravity is tightly related to density, so the density disturbance is supposed to be the most dominant factor. But it seems not the case illustrated by the numerical result. This apparently paradox can be attributed to the fact that density disturbance is lower than that of seismic velocity by a factor of approximately 0.2 to 0.5 (Karato, 1993). That also partly explains why Molodenskii and Kramer (1980) ignored the density disturbance effect. The current results suggest that although the density effects are smaller than those of seismic waves, they are of the same level (Fu and Sun, 2007).

Since the effects of density disturbance are smaller than those of velocity disturbances in the condition that the former's input model is smaller than the latter's, what if the three input models share the same model? To verify this, a simple ocean-land model is constructed and then used for evaluating the effects of disturbances, based on an ocean function. The ocean

https://doi.org/10.5194/egusphere-2022-661
Preprint. Discussion started: 3 August 2022
© Author(s) 2022. CC BY 4.0 License.

function is a delta function with values of 1 and 0 for under the ocean and under the continent, respectively (Balmino et al., 1973). The properties (i.e., seismic wave velocities and densities) under the ocean in the model are 5% higher than those under the continent (Fig. 2d). The pattern in Fig. 2d does not strictly show a delta function for the reason that the function has been developed in spherical harmonics up to 8 degree before being plotted.

Figs. 2a-2c illustrate the effects of P-wave velocity disturbance, S-wave velocity disturbance, and density disturbance on semidiurnal gravimetric factors calculated for the ocean-land model. The patterns are principally consistent with the ocean-land model as the value under the ocean is distinct from that under the continent. The effects of P-wave velocity, S-wave velocity, and density range from −1.2% to 1.1%, −0.5% to 0.8%, and −0.9% to 1.6%, respectively. The numerical results demonstrate that when the models are the same, the effects of density disturbance on semidiurnal gravimetric factors are larger than those of seismic wave velocity disturbances.

The three kinds of effects as shown in Figs. 1a-1c can then be summed to obtain the total changes in semidiurnal gravimetric factor resulting from lateral inhomogeneity (Fig. 1d). The change magnitudes range from −0.18% to 0.09%, similar to those calculated by the density model and smaller than those calculated by the seismic wave models. This further confirms that the density disturbance is not the negligible contributors to total changes. This is because the effects of the two kinds of seismic wave velocity disturbance offset each other as while they have similar distributions with opposite signs. Consequently, density disturbance has a non-negligible influence on tidal gravity. The total changes are negative in the central Pacific, central Eurasia, Australia, South America, North America, and west Africa, while they are positive in east Africa, southeast Asia, and northeast Pacific. The largest negative change is in west Africa, whereas the largest positive change is in northeast Pacific (Hawaii). The magnitude of the lateral inhomogeneity effect does not exceed 0.5%, which is the maximum effect of ellipticity on the gravimetric factor and is considered as the limit of three-dimensional effect (Wang, 1997). The pattern shows very good consistency with the two large low shear velocity provinces beneath the Africa and the Pacific (Ritsema et al., 2011).

To further research the effects of lateral inhomogeneity on semidiurnal gravimetric factors, other four three-dimensional Earth models, i.e., SPani (Tesoniero et al., 2015), SEISGLOB2 (Durand et al., 2017), SGLOBE-rani (Chang et al., 2015), and SAW642ANb (Panning et al., 2010) are adopted. Note that some of these models do not contain density model. Consequently, it's necessary to convert the seismic wave velocity disturbances to density disturbance. The approach of Fu and Sun (2007) is followed to derive the density structure. With the same manipulation as that on GyPSuM, the changes in gravimetric factors calculated by other models are obtained (Fig. 3).

Considering the results shown in Figs. 1d and 3, it can be concluded that both the magnitudes and the overall patterns of the changes calculated by various three-dimensional Earth models are very similar. But in light of that the tidal theory is based on perturbation method, even subtle discrepancies between the three-dimensional Earth models may result in remarkable changes of gravimetric factors. Differences are found at few regions (the east Africa, southeast Pacific, south Indian Ocean, and Tibetan Plateau). For instance, the magnitude at the Tibetan Plateau calculated by the SPani (Fig. 3a) is much larger than that calculated by the GyPSuM (Fig. 1d). Sun et al. (2019) found that the special tectonic setting in the Tibetan Plateau has a

https://doi.org/10.5194/egusphere-2022-661
Preprint. Discussion started: 3 August 2022
© Author(s) 2022. CC BY 4.0 License.

significant influence on tidal gravimetric factors, which means that the result calculated by SPani is more convincible. The lithosphere stresses evaluated by Wang et al. (2015) also confirm that the SPani has a better fitness with observations than the GyPSuM in the Tibetan Plateau. Furthermore, maximum negative values are found at Africa and the Pacific (Fig. 3a), where the two large low shear velocity provinces might locate. The results indicate that tidal tomography contribute to constrain Earth's deep structure (Lau et al., 2017; Wang, 1991). Despite the fact that Fu and Sun (2007) used a relatively old Earth model, close agreement between the current results and Fu and Sun's (2007) results are found (Appendix F). Compared to the results of Fu and Sun (2007), the pattern of this study is more consistent with the distribution of tectonic zones. In particular, relatively large magnitudes are found at major subduction belts (the southeast Asia and west North America) and seismic wave low-velocity anomalies (Africa and the Pacific). Besides, the pattern of this study, to a certain extent, is consistent with the upper mantle results of Métivier and Conrad (2008). The total results of Métivier and Conrad (2008) are more closely related to the large-scale geodynamics activities because they considered dynamic topography.

6.2 Global Distribution of the Theoretical Semidiurnal Tidal Gravity

In order to explore the effects of lateral inhomogeneity on tidal gravity (rather than gravimetric factors), the semidiurnal gravity changes are computed with one-dimensional tidal theory and three-dimensional theory, respectively. In one-dimensional tidal theory, the gravity change caused by tide-generating potential can be presented by the following expression.

$$\Delta g_0(\theta,\phi,t) = \frac{2V_0}{a}\delta_{n_0}P_{n_0}^{m_0}(\cos\theta)\cos(\sigma t - m_0\phi) \tag{51}$$

In three-dimensional tidal theory, the gravity change caused by seismic wave velocity disturbance and density disturbance can be written as

$$\Delta g_{3-D}(\theta,\phi,t) = \frac{2V_0}{a}\sum_{l=0}^{N_e}\sum_{p=-l}^{l}\{\Delta \mathrm{g}_1(\theta,\phi)\cos m_0\phi + \Delta \mathrm{g}_2(\theta,\phi)\sin m_0\phi\}\cos(\sigma t - m_0\phi) \tag{52}$$

where, $\Delta \mathrm{g}_1(\theta,\phi)$ and $\Delta \mathrm{g}_2(\theta,\phi)$ are defined in Equation (49). To observe the maximum effects of lateral inhomogeneity, let's take $\cos(\sigma t - m_0\phi) = 1$, then Equation (52) is simplified as

$$\Delta g_{3-D}(\theta,\phi) = \frac{2V_0}{a}\sum_{l=0}^{N_e}\sum_{p=-l}^{l}\{\Delta \mathrm{g}_1(\theta,\phi)\cos m_0\phi + \Delta \mathrm{g}_2(\theta,\phi)\sin m_0\phi\} \tag{53}$$

Aiming at comparing the differences between the Δg_0 and Δg_{3-D}, it's assumed that $\frac{2V_0}{a} = 1$ and $t = 0$ for simplicity in the numerical process. Basing on the PREM and the GyPSuM, semi-diurnal tidal gravity changes resulted from tide-generating potential and lateral inhomogeneity are calculated, respectively (Fig. 4). The results indicate that the gravity variations attributed to the disturbance are about 0.16% compared with those attributed to the one-dimensional tide-generating potential. Both current and Wang's (1991) results show negative values at the central Pacific and positive values at the east Africa and

https://doi.org/10.5194/egusphere-2022-661
Preprint. Discussion started: 3 August 2022
© Author(s) 2022. CC BY 4.0 License.

southeast Asia. Whereas discrepancies between the two studies exist at the South America and Atlantic, resulted by different Earth models and Wang's (1991) consideration of other factors which may affect the tidal gravity.

Analogous to the research on gravimetric factors, the gravity changes are calculated with uses of different three-dimensional Earth models as well (Fig. 5). Basically, the results calculated by all five three-dimensional Earth models are characterized by positive values at the east Africa, southeast Asia, northeast Pacific, and north Atlantic, and negative values at the west Africa, Australia, and South America. Besides the patterns, the magnitudes of the results calculated by different models are very close as well, varying from -0.0048 to 0.0037. Métivier and Conrad (2008) stated that the effects of mantle heterogeneities on body tides are of order 1‰, consistent with the current result (no more than 2‰). The deviation may be resulted from the lack of dynamic topography, which would partly diminish the effects of laterally-inhomogeneous density. The effects of dynamic topography shall be considered in further research.

7 Relative Contributions of Lateral Inhomogeneity and Other Effects

Besides the lateral inhomogeneity, inertia and ellipticity, inelasticity, and ocean tide loading contribute to the Earth tide as well. This study tests the importance of these factors on the M2 tidal gravimetric factor. To achieve this, the measurements of 15 superconducting gravimeters located at Boulder (America), Cantley (Canada), Canberra (Australia), Esashi (Japan), Matsushiro (Japan), Syowa (Antarctica), Wuhan (China), Membach (Belgium), Metsahovi (Finland), Potsdam (Germany), Strasbourg (France), Vienna (Austria), Lhasa (China), Lijiang (China), Djougou (Benin) are collected (Boy et al., 2003; Hinderer et al., 2020; Sun et al., 2019). The station information and corresponding M2 factors are listed in Table 1.

δ_m in Table 1 is the measured M2 tidal gravimetric factor. All of these measurements are extracted from gravity records longer than two years. $\Delta\delta_e$ is the M2 factor's change resulting from rotation and ellipticity respective to the layered Earth, corresponds to the latitude dependence of the gravimetric factor (Dehant et al., 1999). The $\Delta\delta_e$ results are in good agreement with Wang's (1994) quasi-constant effect of inertia and ellipticity on Earth tides, which is 0.00395. $\Delta\delta_{3D}$, namely, δ_1 in Equation (49), is the M2 factor's change resulting from three-dimensional lateral inhomogeneity, calculated by the GyPSuM model.

According to Table 1, $\Delta\delta_{3D}$ at most stations are one magnitude larger than the errors, indicates that these effects can be detected by superconducting gravimeters and tidal analysis, without considering the poorly understood noise. $\Delta\delta_{3D}$ at European stations are generally very small, consistent with the small tide anomalies reported by Métivier and Conrad (2008), especially for Membach and Metsahovi, where the $\Delta\delta_{3D}$ are basically at the same level with error. Djougou and Syowa show the largest $\Delta\delta_{3D}$. The former may be affected by the large low shear velocity province beneath the Africa, whereas the latter may be partly resulted from polar effects. The largest $\Delta\delta_{3D}$ value is about 1/3 of $\Delta\delta_e$, indicates that the rotation and ellipticity on semidiurnal gravimetric factor should be the major factor to be considered, and the lateral inhomogeneity is the minor but not negligible factor.

https://doi.org/10.5194/egusphere-2022-661
Preprint. Discussion started: 3 August 2022
© Author(s) 2022. CC BY 4.0 License.

Besides the tidal gravity changes for a single instant in time (Figs. 4 and 5), evolution of tidal signals are presented to compare the relative contributions of lateral inhomogeneity and other effects (Fig. 6). The time evolution of four stations are predicted with the use of Tsoft tide-generating program (Van Camp and Vauterin, 2005). These selected stations are Boulder (central North America, the first column in Fig. 6), Syowa (Antarctica, the second column in Fig. 6), Lhasa (Tibetan Plateau, the third column in Fig. 6), and Djougou (west Africa, the forth column in Fig. 6). The time evolution is from September 1st to 16th, close to the equinox, when the tidal gravity is supposed to be the maximum. The tidal gravity shown in the first row in Fig. 6 is synthetized by the observed gravimetric factors reported by previous studies (Boy et al., 2003; Hinderer et al., 2020; Sun et al., 2019). The second row in Fig. 6 presents the gravity difference between DDW99 theoretical tide (Dehant et al., 1999) and a spherical non-rotating elastic isotropic Earth's tide (PREM), corresponds to the effects of rotation, ellipticity, inelasticity, non-hydrostatic structure, and other relative effects. The third row in Fig. 6 presents the ocean tide loading effect calculated by the latest version of the TPXO9-atlas model (https://www.tpxo.net/global/tpxo9-atlas). The fourth row in Fig. 6 illustrates the lateral inhomogeneity effect calculated by the SPani model.

The observed tidal gravity basically varies from -1200 to 1000 nm/s^{-2}. The Syowa and Djougou, where locate in the polar and equatorial band, respectively, have the smallest and largest amplitudes (Figs. 6b and 6d). The effects of rotation, ellipticity, inelasticity, and non-hydrostatic structure are about tens of nm/s^{-2}. Attributed to the very high latitude, the Syowa has the most significant rotation and ellipticity effect (Fig. 6f). Besides, Syowa is the station most affected by the ocean tide loading (Fig. 6j), the effect is up to nearly 70 nm/s^{-2}. Conversely, Lhasa is almost unaffected by the ocean tide (Fig. 6k), compared with the other stations, the effect is only several nm/s^{-2}. As for the lateral inhomogeneity effect, Figs. 6m and 6n suggest that the effect is about 0.05% of the total tidal signal in regions where seismic wave velocity and density anomalies are not very large, such as Boulder and Syowa. For Lhasa and Djougou, where has very special tectonic setting and significantly laterally-inhomogeneous structure, the effect is about 0.1% of the total magnitude (Figs. 6o and 6p). The amplitudes of lateral inhomogeneity are in good coherence of the <1‰ result of Métivier and Conrad (2008), although the current study excludes the effect of dynamic topography. The results shown in Fig. 6 indicate that the rotation, ellipticity, inelasticity, and non-hydrostatic structure on tidal gravity are the most dominant factors, the ocean tide loading should be a moderate factor, and the lateral inhomogeneity is the least but not negligible factor, for the reason that the lateral inhomogeneity effect is comparable with ocean tide loading at some locations. Moreover, the amplitude of tidal gravity caused by lateral inhomogeneity is noticeable larger than the precision of superconducting gravimeters (Rosat and Hinderer, 2018).

8 Conclusions

Three-dimensional tidal theory has been well developed in analytical approach by Fu and Sun (2007), Molodenskiy (1980), Wang (1991), and others. The present study develops the theory by reformulating the expressions and supplementing some critical derivation process. The present study calculates changes to semidiurnal tidal gravimetric factors using the three-

https://doi.org/10.5194/egusphere-2022-661
Preprint. Discussion started: 3 August 2022
© Author(s) 2022. CC BY 4.0 License.

dimensional Earth models (GyPSuM, SPani, SEISGLOB2, SGLOBE-rani, and SAW64ANb). The results calculated by the ocean-land model indicate that the effects of seismic wave velocity disturbance, and density disturbance are at the same level when the same input Earth model is used. Within the results of GyPSuM, the changes to the gravimetric factor resulting from the lateral inhomogeneity of P-wave velocity, S-wave velocity, and density are in the ranges of −0.24% to 0.32%, −0.33% to 0.21%, and −0.12% to 0.09%, respectively. When adding the three kinds of contributions, the total changes to the gravimetric factor are obtained. The total changes are negative in the central Pacific, central Eurasia, Australia, North America, South America, and Africa, and positive in east Africa, southeast Asia, and northeast Pacific. The changes vary from −0.18% to 0.09% (-0.22% to 0.17% for other three-dimensional Earth models) compared with the values of a one-dimensional Earth model. The effects of P-wave velocity disturbance and S-wave velocity disturbance offset each other as while they have similar distributions with opposite signs. Consequently, density disturbance has a non-negligible influence on tidal gravimetric factor.

Besides the gravimetric factor, this work studies the tidal gravity change caused by laterally-inhomogeneous disturbance as well. The results indicate that the maximum gravity variations attributed to the disturbance are about 0.16% compared with those attributed to the one-dimensional tide-generating potential. The gravity change results show positive values at the east Africa, southeast Asia, northeast Pacific, and north Atlantic, and negative values at the west Africa, Australia, and South America. Although the magnitude of the gravity change is similar to that of Métivier and Conrad (2008), the pattern cannot be all the same with their result. The lack of dynamic topography in this study may account for the difference, and it shall be taken into consideration in further research.

Furthermore, this study tests the importance of lateral inhomogeneity and other factors, namely, inertia and ellipticity, inelasticity, and ocean tide loading, on the M2 tidal gravimetric factor and tidal gravity. The maximum M2 factor variation caused by perturbation is about 1/3 of the ellipticity's effect, indicates that the rotation and ellipticity on semidiurnal gravimetric factor should be the major factor, and the lateral inhomogeneity is the minor but not negligible factor. The tidal gravity variations due to lateral inhomogeneity are about 0.05% to 0.1% of the observed signal, namely, about 0.5 to 2 nm/s^{-2}, significantly larger than the precision of superconducting gravimeters.

Data Availability

The three-dimensional Earth models can be found on IRIS website (see http://ds.iris.edu/ds/products/emc-Earthmodels/). The ocean tide loading effect can be calculated on OTL provider website (see http://holt.oso.chalmers.se/loading/).

Author contributions

ZW conceptualized the project and made the mathematical and software development. ZW conceived, designed, and performed the experiments. ZW analysed the result and drafted the manuscript. ZW procured funding.

https://doi.org/10.5194/egusphere-2022-661
Preprint. Discussion started: 3 August 2022
© Author(s) 2022. CC BY 4.0 License.

Competing interests

The contact author has declared no competing interests.

Acknowledgments

Thanks to Professor R. Wang and Professor L. Métivier for valuable comments, and Professor G. Fu for helpful discussions. The author received funding from the Special Fund of the Institute of Earthquake Forecasting, China Earthquake Administration (CEAIEF20220212).

Financial support

The project was supported by the Special Fund of the Institute of Earthquake Forecasting, China Earthquake Administration (CEAIEF20220212).

Appendix A: Algorithms for Coefficients $y_i(r)$

Determining coefficients $y_i(r), i = 1, \dots, 6$ is the key process to obtain the solutions of Love numbers and Green's functions. The explicit expressions for calculating $y_i(r)$ have been presented by many researchers (Longman, 1963; Sun and Okubo, 1993; Wang et al., 2012). Although deviations of definitions and treatments exist in different papers, the final results are basically the same. Here the expressions proposed by Longman (1963) are addressed. According to definition, $y_i(r)$ satisfies:

$$\dot{y}_1(r) = -\frac{2\lambda}{\lambda+2\mu}\frac{y_1(r)}{r} + \frac{y_2(r)}{\lambda+2\mu} + n(n+1)\frac{\lambda}{\lambda+2\mu}\frac{y_3(r)}{r} \tag{A1}$$

$$\dot{y}_2(r) = \left[-4C\rho gr + \frac{4\mu(3\lambda+2\mu)}{\lambda+2\mu}\right]\frac{y_1(r)}{r^2} - \frac{4\mu}{\lambda+2\mu}\frac{y_2(r)}{r} + n(n+1)\left[C\rho gr - \frac{2\mu(3\lambda+2\mu)}{\lambda+2\mu}\right]\frac{y_3(r)}{r^2} + n(n+1)\frac{y_4(r)}{r} - C\rho y_6(r) \tag{A2}$$

$$\dot{y}_3(r) = -\frac{y_1(r)}{r} + \frac{y_3(r)}{r} + \frac{y_4(r)}{\mu} \tag{A3}$$

$$\dot{y}_4(r) = \left[C\rho gr - \frac{2\mu(3\lambda+2\mu)}{\lambda+2\mu}\right]\frac{y_1(r)}{r^2} - \frac{\lambda}{\lambda+2\mu}\frac{y_2(r)}{r} + \frac{2\mu}{\lambda+2\mu}[\lambda(2n^2+2n-1) + 2\mu(2n^2+2n-1)]\frac{y_3(r)}{r^2} - 3\frac{y_4(r)}{r} - C\rho\frac{y_5(r)}{r} \tag{A4}$$

$$\dot{y}_5(r) = B\rho y_1(r) + y_6(r) \tag{A5}$$

$$\dot{y}_6(r) = -n(n+1)B\rho\frac{y_3(r)}{r} + n(n+1)B\rho\frac{y_5(r)}{r^2} - 2\frac{y_6(r)}{r} \tag{A6}$$

In Equations (A1) - (A6),

https://doi.org/10.5194/egusphere-2022-661
Preprint. Discussion started: 3 August 2022
© Author(s) 2022. CC BY 4.0 License.

$$\begin{cases} B = 4\pi G\rho_0 a/g_0 \\ C = \rho_0 g_0 a/\lambda_0 \end{cases} \tag{A7}$$

G is Newton's gravitational constant, ρ_0 and λ_0 are density and rheology parameter at the centre of Earth, a and g_0 are radius and gravity on the surface of Earth. $y_i(r)$ can be determined by integrating the differential equations from initial value to surface by Runge-Kutta method (Longman, 1963), with the help of following boundary conditions,

$$\begin{cases} y_2(a) = 0 \\ y_4(a) = 0 \\ y_6(a) + (n+1)y_5(a) = 2n+1 \end{cases} \tag{A8}$$

Appendix B: Treatment of integral *I*

The expression I is an integral of combination of perturbation solution and auxiliary solution $u_i^j L_i(\delta\boldsymbol{u}, \delta\Psi) - \delta u_i L_i(\boldsymbol{u}^j, \Psi^j)$. Equation (26) may be reduced to a surface integral by integrating by parts:

$$\begin{aligned} I = \iiint \Bigg[& \frac{\partial}{\partial x_k}\left(u_i^j \delta\tau_{ik} - \delta u_i \tau_{ik}^j\right) - \delta\tau_{ik}\frac{\partial u_i^j}{\partial x_k} + \tau_{ik}^j \frac{\partial \delta u_i}{\partial x_k} + \frac{\partial}{\partial x_i}\left(\rho u_i^j \psi^* - \rho\delta u_i \psi^j\right) - \psi^* \frac{\partial}{\partial x_i}\left(\rho u_i^j\right) + \psi^j \frac{\partial}{\partial x_i}(\rho\delta u_i) \\ & + \delta u_i \frac{\partial}{\partial x_i}(\rho \boldsymbol{u}^j, \nabla V) - u_i^j \frac{\partial}{\partial x_i}(\rho\delta\mathbf{u}, \nabla V) \Bigg] dv \\ = & \iint \left(u_i^j \delta\tau_{ik} - \delta u_i \tau_{ik}^j + \rho u_k^j \psi^* - \rho\delta u_k \psi^j\right) dS_k \\ & + \iiint \left[\Psi^j(\rho\nabla_i \delta u_i + \delta u_i \nabla_i \rho) - \delta\Psi\left(\rho\nabla_i u_i^j + u_i^j \nabla_i \rho\right)\right] dv \end{aligned} \tag{B1}$$

where,

$$\delta\tau_{ik} = \mu\left(\frac{\partial \delta u_i}{\partial x_k} + \frac{\partial \delta u_k}{\partial x_i}\right) + \lambda\nabla_i \delta u_i \delta_{ik}$$

$$\tau_{ik}^j = \mu\left(\frac{\partial u_i^j}{\partial x_k} + \frac{\partial u_k^j}{\partial x_i}\right) + \lambda\nabla_i u_i^j \delta_{ik}$$

$$\psi^* = \delta\Psi + \delta u_i \nabla_i V$$

$$\psi^j = \Psi^j + u_i^j \nabla_i V$$

$$dS_k = \frac{x_k}{r} dS$$

By using the condition of zero stress on the surface for the initial and perturbed boundary problems, it's obtained that

$$\delta\tau_{ik}|_S = -\left[\delta\mu\left(\frac{\partial u_i^0}{\partial x_k} + \frac{\partial u_k^0}{\partial x_i}\right) + \delta\lambda\nabla\cdot(\boldsymbol{u}^0)\delta_{ik}\right]\Big|_S$$

Note that the expression of $\delta\tau_{ik}$ here is different from $\delta\tau_{ik}$ in a volume integration. The "·" denotes scalar product.

The remaining volume integral in Equation (B1) may be transformed by applying Poisson's equation (Equation 3) for the solution u_i^j and Ψ^j:

https://doi.org/10.5194/egusphere-2022-661
Preprint. Discussion started: 3 August 2022
© Author(s) 2022. CC BY 4.0 License.

$$\rho\nabla_i u_i^j + (\boldsymbol{u}^j, \nabla\rho) = \frac{1}{4\pi G}\nabla^2\Psi^j \tag{B2}$$

and the result of varying Equation (3)

$$\rho\nabla_i \delta u_i + (\delta\boldsymbol{u}, \nabla\rho) = \frac{1}{4\pi G}\nabla^2(\delta\Psi) - \nabla_i u_i^0\delta\rho - (\boldsymbol{u}^0, \nabla\delta\rho) \tag{B3}$$

By substituting Equations (B2) and (B3) into the last term of Equation (B1), this integral transforms to

$$\iiint \left[\frac{1}{4\pi G}(\Psi^j\nabla^2(\delta\Psi) - \delta\Psi\nabla^2\Psi^j) - \Psi^j\left(\delta\rho\nabla_i u_i^0 + (\boldsymbol{u}^0, \nabla\delta\rho)\right)\right] dv \tag{B4}$$

The first term in Equation (B4) can be reduced to a surface integral by means of Green's formula

$$\iiint (\Psi^j\nabla^2(\delta\Psi) - \delta\Psi\nabla^2\Psi^j)\, dv = \iint \left(\Psi^j\frac{\partial(\delta\Psi)}{\partial n} - \delta\Psi\frac{\partial\Psi^j}{\partial n}\right) dS \tag{B5}$$

where $\frac{\partial}{\partial n}$ indicates a derivative with regard to the external normal. The second term does not contain any variations of solutions and may be considered as a known quantity.

Now, let's express the remaining surface integrals in Equation (B1) in terms of variations of coefficients $y_i(r)$. The integrand of the first term in Equation (B1) may be written as follows:

$$\left(u_i^j\delta\tau_{ik} - \delta u_i\tau_{ik}^j\right)\frac{x_k}{r} = u_i^j\frac{x_k}{r}\delta\tau_{ik} - \frac{\delta u_i}{r}\left\{\mu\left[\left(x_k, \nabla_k u_i^j\right) + \nabla_i\left(x_k, u_k^j\right) - u_k^j\delta_{ik}\right] + \lambda x_k\nabla_i u_i^j\delta_{ik}\right\} \tag{B6}$$

Let us choose the auxiliary solutions u_i^j and Ψ^j of unperturbed equations (Equations 22 and 23) proportional to a spherical function of the degree n:

$$\boldsymbol{u}^j = \sum_{n=0}^{\infty}\sum_{m=-n}^{n}\left[y_1^j(r;n,m)\boldsymbol{R}_n^m(\theta,\phi) + y_3^j(r;n,m)\boldsymbol{S}_n^m(\theta,\phi)\right] \tag{B7}$$

$$\Psi^j = \sum_{n=0}^{\infty}\sum_{m=-n}^{n} y_5^j(r;n,m)Y_n^m(\theta,\phi) \tag{B8}$$

The index $j = 1,2,3$ will give the number of the regular (toward the center) solution (Equations B7 and B8) with fixed n, m. By substituting Eqs (18), (19), (B7), and (B8) into Equation (B1), considering Equations (B4), (B5), and (B6), and integrating the terms not containing density variations and Lame's parameters with respect to angular variables, Equation (B9) is obtained.

$$I = \frac{4\pi(n+m)!}{\varepsilon_m(2n+1)(n-m)!}$$
$$\cdot\left\{-y_1^*(1;n,m)y_2^j(1) - n(n+1)y_3^*(1;n,m)y_4^j(1) + \frac{1}{4\pi G}\left[y_6^*(1;n,m)y_5^j(1) - y_5^*(1;n,m)y_6^j(1)\right]\right\}$$
$$-\iiint \Psi^j\nabla\cdot(\delta\rho\boldsymbol{u}^0)\, dv + \iint\left(u_i^j\delta\tau_{ik} + \Psi^j u_k^0\delta\rho\right)dS_k \tag{B9}$$

where,

https://doi.org/10.5194/egusphere-2022-661
Preprint. Discussion started: 3 August 2022
© Author(s) 2022. CC BY 4.0 License.

$$y_2^j(r) = (\lambda + 2\mu)\dot{y}_1^j(r) + \frac{\lambda}{r}\left[2y_1^j(r) - n(n+1)y_3^j(r)\right]$$

$$y_4^j(r) = \frac{\mu}{r}\left[y_1^j(r) - y_3^j(r) + r\dot{y}_3^j(r)\right]$$

$$y_6^j(r) = \dot{y}_5^j(r) - 4\pi G\rho y_1^j(r)$$

$$y_6^*(r) = \dot{y}_5^*(r) - 4\pi G\rho y_1^*(r) - 4\pi G\delta\rho y_1^0(r)$$

The following orthogonality properties of the gradients of the spherical functions are taken into consideration in Equation (B9).

$$\iint \left(\nabla_i Y_n^m(\theta,\phi), \nabla_i Y_k^l(\theta,\phi)\right) dS = \frac{4\pi(n+m)!}{\varepsilon_m(2n+1)(n-m)!} n(n+1)\delta_{nk}\delta_{ml} \tag{B10}$$

where,

$$\varepsilon_m = \begin{cases} 1 & m = 0 \\ 2 & m \neq 0 \end{cases}$$

Now let us apply the boundary conditions for the variation of the surface potential for a tide of order n

$$(n+1)y_5^0(1) + y_6^0(1) = 2n + 1 \tag{B11}$$

By varying Equation (B11) the uniform boundary conditions for solution variations are obtained

$$(n+1)y_5^*(1) + y_6^*(1) = 0 \tag{B12}$$

$$y_6^*(1;n,m)y_5^j(1) - y_5^*(1;n,m)y_6^j(1) = -y_5^*(1;n,m)\left[(n+1)y_5^j(1) + y_6^j(1)\right] \tag{B13}$$

Substituting Equation (B13) into Equation (B9) yields Equation (27).

Appendix C: Treatment of $A_{lpnmn_0m_0}$

Equation (39) can be written as:

$$A_{lpnmn_0m_0} = \iint Y_l^p(\theta,\phi)Y_n^m(\theta,\phi)Y_{n_0}^{m_0}(\theta,\phi)dS = E_{lpnmn_0m_0}I(p,m,m_0) \tag{C1}$$

$$E_{lpnmn_0m_0} = \int_{-\frac{\pi}{2}}^{\frac{\pi}{2}} P_l^p(\cos\theta)P_n^m(\cos\theta)P_{n_0}^{m_0}(\cos\theta)d\theta \tag{C2}$$

$$I(p,m,m_0) = \int_0^{2\pi} \begin{cases}\cos p\phi \\ \sin p\phi\end{cases}\begin{cases}\cos m\phi \\ \sin m\phi\end{cases}\begin{cases}\cos m_0\phi \\ \sin m_0\phi\end{cases} d\phi \tag{C3}$$

In light of Fu and Sun (2008), the normalized form of $E_{lpnmn_0m_0}$ is

$$\bar{E}_{lpnmn_0m_0} = 4\sqrt{2}(-1)^p(2l+1)^{1/2}(2n+1)^{1/2}(2n_0+1)^{1/2}\begin{pmatrix} l & n & n_0 \\ -p & m & m_0\end{pmatrix}\begin{pmatrix} l & n & n_0 \\ 0 & 0 & 0\end{pmatrix} \tag{C4}$$

The value of $\bar{E}_{lpnmn_0m_0}$ need to divide $\sqrt{2}$ if each of p, m, and m_0 equals 0. The Wigner 3j symbol in Equation (C4) is defined as following.

https://doi.org/10.5194/egusphere-2022-661
Preprint. Discussion started: 3 August 2022
© Author(s) 2022. CC BY 4.0 License.

$$\begin{pmatrix} a & b & c \\ \alpha & \beta & \gamma \end{pmatrix} = (-1)^{a-b-\gamma}\left[\frac{(a+b-c)!\,(a-b+c)!\,(-a+b+c)!}{(a+b+c+1)!}\right]^{\frac{1}{2}}[(a+\alpha)!\,(a-\alpha)!\,(b+\beta)!\,(b-\beta)!\,(c+\gamma)!\,(c-\gamma)!]^{\frac{1}{2}}\sum_k (-1)^k[k!\,(a+b-c-k)!\,(a-\alpha-k)!\,(b+\beta-k)!\,(c-a-\beta-k)!\,(c-b+\alpha+k)!]^{-1} \quad \text{(C5)}$$

The range of k is limited to make sure that all factorials in the denominator are non-negative.

As for $I(p,m,m_0)$,

$$\int_0^{2\pi} \sin m_1\phi \cos m_2\phi \cos m_3\phi\, d\phi = 0 \quad \text{(C6)}$$

$$\int_0^{2\pi} \sin m_1\phi \sin m_2\phi \sin m_3\phi\, d\phi = 0 \quad \text{(C7)}$$

$$\int_0^{2\pi} \cos m_1\phi \cos m_2\phi \cos m_3\phi\, d\phi = \frac{\pi}{2}\left[\delta_{m_1+m_2,m_3} + \delta_{m_2+m_3,m_1} + \delta_{m_1+m_3,m_2} + \delta_{m_1+m_2,-m_3}\right] \quad \text{(C8)}$$

$$\int_0^{2\pi} \sin m_1\phi \cos m_2\phi \sin m_3\phi\, d\phi = \frac{\pi}{2}\left[\delta_{m_2+m_3,m_1} - \delta_{m_1+m_3,m_2} + \delta_{m_1+m_2,m_3} - \delta_{m_1+m_2,-m_3}\right] \quad \text{(C9)}$$

Appendix D: Expressions of $x_{nn_0}^{(i)(j)}(r)$

In Equations (36) and (37),

$$x_{nn_0}^{(1)(j)}(r) = r^2\left[\dot{y}_1^0(r) + \frac{2}{r}y_1^0(r) - \frac{n_0(n_0+1)}{r}y_3^0(r)\right]\cdot\left[\dot{y}_1^j(r) + \frac{2}{r}y_1^j(r) - \frac{n(n+1)}{r}y_3^j(r)\right] \quad \text{(D1)}$$

$$x_{nn_0}^{(2)(j)}(r) = 2r^2\left\{r^2\dot{H}_n^j\dot{H}_{n_0} + r\dot{H}_n^jH_{n_0} + rH_n^j\dot{H}_{n_0} + nr\dot{H}_{n_0}\left(H_n^j + \frac{\dot{T}_n^j}{r}\right) + n_0r\dot{H}_n^j\left(H_{n_0} + \frac{\dot{T}_{n_0}}{r}\right) + \frac{n(n-1)}{r}\dot{H}_{n_0}T_n^j + \frac{n_0(n_0-1)}{r}\dot{H}_n^jT_{n_0} + 3H_n^jH_{n_0} + nH_{n_0}\left(H_n^j + \frac{\dot{T}_n^j}{r}\right) + n_0H_n^j\left(H_{n_0} + \frac{\dot{T}_{n_0}}{r}\right) + \frac{nn_0}{2}\left(H_{n_0} + \frac{\dot{T}_{n_0}}{r}\right)\left(H_n^j + \frac{\dot{T}_n^j}{r}\right)\right\} \quad \text{(D2)}$$

$$x_{nn_0}^{(3)(j)}(r) = \left\{r^2\left(H_{n_0} + \frac{\dot{T}_{n_0}}{r}\right)\left(H_n^j + \frac{\dot{T}_n^j}{r}\right) + 2(n-1)T_n^j\left(H_{n_0} + \frac{\dot{T}_{n_0}}{r}\right) + 2(n_0-1)T_{n_0}\left(H_n^j + \frac{\dot{T}_n^j}{r}\right)\right\} \quad \text{(D3)}$$

$$x_{nn_0}^{(4)(j)}(r) = \frac{2}{r^2}T_n^jT_{n_0} \quad \text{(D4)}$$

In Equations (D2) - (D4):

$$H_n^j = \frac{y_1^j(r)}{r^{n+1}} - \frac{ny_3^j(r)}{r^{n+1}};\ T_n^j = \frac{y_3^j(r)}{r^{n-1}}$$

https://doi.org/10.5194/egusphere-2022-661
Preprint. Discussion started: 3 August 2022
© Author(s) 2022. CC BY 4.0 License.

$$H_{n_0}(r) = \frac{y_1^0(r)}{r^{n_0+1}} - \frac{n_0 y_3^0(r)}{r^{n_0+1}};\ T_{n_0}(r) = \frac{y_3^0(r)}{r^{n_0-1}} \tag{D5}$$

In Equation (38),

$$x_{nn_0}^{(5)(j)}(r) = r^{n+n_0+2}\left[h_{n_0}^0(r)h_n^1(r) + h_n^j(r)h_{n_0}^4(r) + g(r)h_n^j(r)h_{n_0}^2(r)\right] - g(r)r^2 y_1^j(r)D_{n_0}(r) \tag{D6}$$

$$x_{nn_0}^{(6)(j)}(r) = r^{n+n_0}\left[t_{n_0}^0(r)t_n^1(r) + t_n^j(r)t_{n_0}^4(r) + g(r)t_n^j(r)t_{n_0}^2(r)\right] \tag{D7}$$

$$x_{nn_0}^{(7)(j)}(r) = r^{n+n_0+2}g(r)h_n^j(r)h_{n_0}^2(r) - g(r)r^2 y_1^j(r)D_{n_0}(r) \tag{D8}$$

$$x_{nn_0}^{(8)(j)}(r) = r^{n+1}g(r)h_n^j(r)y_1^0(r) \tag{D9}$$

$$x_{nn_0}^{(9)(j)}(r) = r^{n+n_0}g(r)t_n^j(r)t_{n_0}^2(r) \tag{D10}$$

$$x_{nn_0}^{(10)(j)}(r) = r^n g(r)t_n^j(r)y_1^0(r) \tag{D11}$$

$$x_{nn_0}^{(11)(j)}(r) = r^{n+2}\dot{g}(r)h_n^j(r)y_1^0(r) \tag{D12}$$

where,

$$D_{n_0}(r) = \dot{y}_1^0(r) + \frac{2}{r}y_1^0(r) - \frac{n_0(n_0+1)}{r}y_3^0(r) \tag{D13}$$

$$h_{n_0}^0(r) = \frac{y_1^0(r)}{r^{n_0}} - \frac{n_0 y_3^0(r)}{r^{n_0}};\ t_{n_0}^0(r) = \frac{y_3^0(r)}{r^{n_0-1}} \tag{D14}$$

$$h_n^j(r) = \frac{y_1^j(r)}{r^n} - \frac{n y_3^j(r)}{r^n};\ t_n^j(r) = \frac{y_3^j(r)}{r^{n-1}} \tag{D15}$$

$$h_n^1(r) = \frac{\dot{y}_5^j(r)}{r^n} - \frac{n y_5^j(r)}{r^{n+1}};\ t_n^1(r) = \frac{y_5^j(r)}{r^n} \tag{D16}$$

$$h_{n_0}^2(r) = \frac{\dot{y}_1^0(r)}{r^{n_0}} - \frac{n_0 y_1^0(r)}{r^{n_0+1}};\ t_{n_0}^2(r) = \frac{y_1^0(r)}{r^{n_0}} \tag{D17}$$

$$h_{n_0}^4(r) = \frac{\dot{y}_5^0(r)}{r^{n_0}} - \frac{n_0 y_5^0(r)}{r^{n_0+1}};\ t_{n_0}^4(r) = \frac{y_5^0(r)}{r^{n_0}} \tag{D18}$$

Appendix E: Final Formulae for Effects of Lateral Inhomogeneity

By substituting Equation (33) into Equation (15):

$$\Delta g(\theta,\phi) = \sum_{n=0}^{\infty}\sum_{m=-n}^{n}\frac{1}{c(n,m)}[(n+1)F^{j=3}(\delta\rho,\delta\mu,\delta\lambda) - 2F^{j=1}(\delta\rho,\delta\mu,\delta\lambda)]Y_n^m(\theta,\phi) \tag{E1}$$

The disturbance of λ is taken for example. By substituting Equation (36) into Equation (E1),

$$\begin{aligned}\Delta g_\lambda(\theta,\phi) &= -\sum_{n=0}^{\infty}\sum_{m=-n}^{n}\sum_{l=0}^{N_e}\sum_{p=-l}^{l}\frac{A_{lpnmn_0m_0}}{c(n,m)}Y_n^m(\theta,\phi)\int_0^1\lambda_{lp}(r)\left[(n+1)x_{nn_0}^{(1)(j=3)}(r) - 2x_{nn_0}^{(1)(j=1)}(r)\right]dr \\ &= \sum_{n=0}^{\infty}\sum_{m=-n}^{n}\sum_{l=0}^{N_e}\sum_{p=-l}^{l}\frac{E_{lpnmn_0m_0}}{c(n,m)}I(p,m,m_0)Y_n^m(\theta,\phi)\int_0^1\lambda_{lp}(r)y_n(r)dr\end{aligned} \tag{E2}$$

https://doi.org/10.5194/egusphere-2022-661
Preprint. Discussion started: 3 August 2022
© Author(s) 2022. CC BY 4.0 License.

$$y_n(r) = 2x_{nn_0}^{(1)(j=1)}(r) - (n+1)x_{nn_0}^{(1)(j=3)}(r) \tag{E3}$$

Therein, the treatments on $E_{lpnmn_0m_0}$ and $I(p,m,m_0)$ can be found in Appendix C.

As discussed by Molodenskii and Kramer (1980), $I(p,m,m_0) \neq 0$ only when $p = m \pm m_0$. Besides, $E_{lpnmn_0m_0} = 0$ if l, n, and n_0 do not satisfy a triangle inequality. The integration of dr start from the core-mantle boundary, rather than the core of Earth, to the surface, layer by layer. So the Equation (E2) simplifies as,

$$\Delta g_\lambda(\theta,\phi) = \sum_{l=0}^{N_e}\sum_{p=-l}^{l}\sum_{n=|l-n_0|}^{l+n_0} \frac{E_{lpnmn_0m_0}}{c(n,p\pm m_0)} I(p,p\pm m_0,m_0) Y_n^{p\pm m_0}(\theta,\phi) \int_b^1 \lambda_{lp}(r) y_n(r) dr$$

By replacing $\lambda_{lp}(r)$ with $\alpha_{lp}(r)$, $\beta_{lp}(r)$, and $\gamma_{lp}^1(r)$ with the help of Equation (41):

$$\Delta g_\lambda(\theta,\phi) = \sum_{l=0}^{N_e}\sum_{p=-l}^{l}\sum_{n=|l-n_0|}^{l+n_0} \frac{E_{lpn(p\pm m_0)n_0m_0}}{c(n,p\pm m_0)} I(p,p\pm m_0,m_0) Y_n^{p\pm m_0}(\theta,\phi) \int_b^1 y_n(r)\big[2(\lambda+2\mu)\alpha_{lp}(r) - 4\mu\beta_{lp}(r) + \lambda\gamma_{lp}^1(r)\big] dr \tag{E4}$$

Similarly, the expressions for $\delta\mu$ and $\delta\rho$ are,

$$\Delta g_\mu(\theta,\phi) = \sum_{l=0}^{N_e}\sum_{p=-l}^{l}\sum_{n=|l-n_0|}^{l+n_0} \frac{E_{lpn(p\pm m_0)n_0m_0}}{c(n,p\pm m_0)} I(p,p\pm m_0,m_0) Y_n^{p\pm m_0}(\theta,\phi) \int_b^1 z_n(r)\big[2\mu\beta_{lp}(r) + \mu\gamma_{lp}^1(r)\big] dr \tag{E5}$$

$$\Delta g_\rho(\theta,\phi) = \sum_{l=0}^{N_e}\sum_{p=-l}^{l}\sum_{n=|l-n_0|}^{l+n_0} \frac{E_{lpn(p\pm m_0)n_0m_0}}{c(n,p\pm m_0)} I(p,p\pm m_0,m_0) Y_n^{p\pm m_0}(\theta,\phi) \int_b^1 \rho(r)\big[q_n^1(r)\gamma_{lp}^1(r) + q_n^2(r)\gamma_{lp}^2(r) + q_n^3(r)\gamma_{lp}^3(r)\big] dr \tag{E6}$$

In Equations (E5) and (E6),

$$z_n(r) = r^{n+n_0}\Big[2x_{nn_0}^{(2)(j=1)}(r) - (n+1)x_{nn_0}^{(2)(j=3)}(r) + nn_0\left(2x_{nn_0}^{(3)(j=1)}(r) - (n+1)x_{nn_0}^{(3)(j=3)}(r)\right) + nn_0(nn_0 - n_0 - n + 3)\left(2x_{nn_0}^{(4)(j=1)}(r) - (n+1)x_{nn_0}^{(4)(j=3)}(r)\right)\Big] \tag{E7}$$

$$q_n^1(r) = 2x_{nn_0}^{(5)(j=1)}(r) - (n+1)x_{nn_0}^{(5)(j=3)}(r) + nn_0\left(2x_{nn_0}^{(6)(j=1)}(r) - (n+1)x_{nn_0}^{(6)(j=3)}(r)\right) \tag{E8}$$

$$q_n^2(r) = 2x_{nn_0}^{(7)(j=1)}(r) - (n+1)x_{nn_0}^{(7)(j=3)}(r) - l\left(2x_{nn_0}^{(8)(j=1)}(r) - (n+1)x_{nn_0}^{(8)(j=3)}(r)\right) + nn_0\left(2x_{nn_0}^{(9)(j=1)}(r) - (n+1)x_{nn_0}^{(9)(j=3)}(r)\right) + nl\left(2x_{nn_0}^{(10)(j=1)}(r) - (n+1)x_{nn_0}^{(10)(j=3)}(r)\right) \tag{E9}$$

$$q_n^3(r) = 2x_{nn_0}^{(11)(j=1)}(r) - (n+1)x_{nn_0}^{(11)(j=3)}(r) \tag{E10}$$

Equations (E4) and (E5) can be transformed into the forms relating to seismic wave velocity disturbance, namely Equations (44) and (45).

Appendix F: Comparison with the Results of Fu and Sun (2007)

https://doi.org/10.5194/egusphere-2022-661
Preprint. Discussion started: 3 August 2022
© Author(s) 2022. CC BY 4.0 License.

Fu and Sun (2007) modified the solution presented by Molodenskii and Kramer (1980) and Wang (1991), with the consideration of density disturbance. Compared with the current study, Fu and Sun (2007) adopted a relatively old Earth model with resolution of 5 degree (Zhao, 2001) and directly integrated the product of three Legendre functions to compute $E_{lpnmn_0m_0}$, but not the analytical solution (Equation C4, Fu and Sun, 2008).

As Fig. F1 shows, the changes derived from P-wave velocity disturbance, S-wave velocity disturbance, density disturbance, and total effects are −0.28% to 0.25%, −0.29% to 0.26%, −0.09% to 0.12%, and −0.13% to 0.12%, respectively. The results of Fu and Sun (2007) are generally consistent with the present study (Fig. 1 and Fig. 3) on a global scale. Furthermore, the results calculated by new Earth models show more details.

References

Miller, B. B. and Carter, C.: The test article, J. Sci. Res., 12, 135–147, doi:10.1234/56789, 2015.

Smith, A. A., Carter, C., and Miller, B. B.: More test articles, J. Adv. Res., 35, 13–28, doi:10.2345/67890, 2014.

Balmino, G., Lambeck, K., and Kaula, W. M.: A spherical harmonic analysis of the Earth's topography, Journal of Geophysical Research, 78(2), 478-481, https://doi.org/10.1029/JB078i002p00478, 1973.

Chang, S. J., Ferreira, A. M., Ritsema, J., van Heijst, H. J., and Woodhouse, J. H.: Joint inversion for global isotropic and radially anisotropic mantle structure including crustal thickness perturbations, Journal of Geophysical Research: Solid Earth, 120(6), 4278-4300, https://doi.org/10.1002/2014JB011824, 2015.

Dahlen, F. A.: Elastic dislocation theory for a self-gravitating elastic configuration with an initial static stress field, Geophysical Journal International, 28(4), 357-383, https://doi.org/10.1111/j.1365-246X.1972.tb06798.x, 1972.

Dahlen, F. and Tromp, J.: Theoretical global seismology, Princeton university press, 2021.

Dehant, V.: Tidal parameters for an inelastic Earth, Physics of the Earth and Planetary Interiors, 49(1-2), 97-116, https://doi.org/10.1016/0031-9201(87)90134-8, 1987.

Dehant, V., Defraigne, P., and Wahr, J. M.: Tides for a convective Earth, Journal of Geophysical Research: Solid Earth, 104(B1), 1035-1058, https://doi.org/10.1029/1998JB900051, 1999.

de Vries, D. and Wahr, J. M.: The effects of the solid inner core and non-hydrostatic structure on the Earth's forced nutations and Earth tides, Journal of Geophysical Research: Solid Earth, 96(B5), 8275-8293, https://doi.org/10.1029/90JB01958, 1991.

Durand, S., Debayle, E., Ricard, Y., Zaroli, C., and Lambotte, S.: Confirmation of a change in the global shear velocity pattern at around 1000 km depth, Geophysical Journal International, 211(3), 1628-1639, https://doi.org/10.1093/gji/ggx405, 2017.

Dziewonski, A. M. and Anderson, D. L.: Preliminary reference Earth model, Physics of the Earth and Planetary Interiors, 25(4), 297-356, doi: 10.1016/0031- 9201(81)90046-7, 1981.

https://doi.org/10.5194/egusphere-2022-661
Preprint. Discussion started: 3 August 2022
© Author(s) 2022. CC BY 4.0 License.

Farrell, W. E.: Deformation of the Earth by surface loads, Reviews of Geophysics, 10(3), 761-797, https://doi.org/10.1029/RG010i003p00761, 1972.

Fu, G. and Sun, W.: Effects of lateral inhomogeneity in a spherical Earth on gravity Earth tides, Journal of Geophysical Research: Solid Earth, 112(B6), https://doi.org/10.1029/2006JB004512, 2007.

Fu, G. and Sun, W.: Surface coseismic gravity changes caused by dislocations in a three-dimensional heterogeneous Earth, Geophysical Journal International, 172(2), 479-503, https://doi.org/10.1111/j.1365-246X.2007.03684.x, 2008.

Geller, R. J.: Elastodynamics in a laterally heterogeneous, self-gravitating body, Geophysical Journal International, 94(2), 271-283, https://doi.org/10.1111/j.1365-246X.1988.tb05901.x, 1988.

Karato, S. I.: Importance of anelasticity in the interpretation of seismic tomography, Geophysical Research Letters, 20(15), 1623-1626, https://doi.org/10.1029/93GL01767, 1993.

Lau, H. C. and Faul, U. H.: Anelasticity from seismic to tidal timescales: Theory and observations, Earth and Planetary Science Letters, 508, 18-29, https://doi.org/10.1016/j.epsl.2018.12.009, 2019.

Lau, H. C., Mitrovica, J. X., Davis, J. L., Tromp, J., Yang, H. Y., and Al-Attar, D.: Tidal tomography constrains Earth's deep-mantle buoyancy, Nature, 551(7680), 321-326, https://doi.org/10.1038/nature24452, 2017.

Lau, H. C., Yang, H. Y., Tromp, J., Mitrovica, J. X., Latychev, K., and Al-Attar, D.: A normal mode treatment of semi-diurnal body tides on an aspherical, rotating and anelastic Earth, Geophysical Journal International, 202(2), 1392-1406, doi: 10.1093/gji/ggv227, 2015.

Longman, I. M.: A Green's function for determining the deformation of the Earth under surface mass loads: 2. computations and numerical results, Journal of Geophysical Research, 68(2), 485-496, https://doi.org/10.1029/JZ068i002p00485, 1963.

Love, A. E. H.: The yielding of the Earth to disturbing forces, Proceedings of the Royal Society A, Mathematical, Physical and Engineering Sciences, 82(551), 73-88, https://doi.org/10.1098/rspa.1909.0008, 1909.

Métivier, L. and Conrad, C. P.: Body tides of a convecting, laterally heterogeneous, and aspherical Earth, Journal of Geophysical Research: Solid Earth, 113(B11), https://doi.org/10.1029/2007JB005448, 2008.

Métivier, L., Greff-Lefftz, M., and Diament, M.: Mantle lateral variations and elastogravitational deformations–I. Numerical modelling, Geophysical Journal International, 167(3), 1060-1076, https://doi.org/10.1111/j.1365-246X.2006.03159.x, 2006.

Métivier, L., Greff-Lefftz, M., and Diament, M.: Mantle lateral variations and elastogravitational deformations–II. Possible effects of a superplume on body tides, Geophysical Journal International, 168(3), 897-903, https://doi.org/10.1111/j.1365-246X.2006.03309.x, 2007.

Molodenskiy, S. M.: The influence of horizontal inhomogeneities in the mantle on the amplitude of tidal oscillations, Izvestiya, Physics of the Solid Earth, 13, 77-80, 1977.

Molodenskiy, S. M.: The effect of lateral heterogeneities upon the tides, BIM Fevrier, 80, 4833-4850, 1980.

Molodenskii, S. M. and Kramer, M. V.: The influence of large-scale horizontal inhomogeneities in the mantle on Earth tides, Izvestiya, Earth Physics, 16, 1-11, 1980.

https://doi.org/10.5194/egusphere-2022-661
Preprint. Discussion started: 3 August 2022
© Author(s) 2022. CC BY 4.0 License.

Panning, M. P., Lekić, V., and Romanowicz, B. A.: Importance of crustal corrections in the development of a new global model of radial anisotropy, Journal of Geophysical Research: Solid Earth, 115(B12), https://doi.org/10.1029/2010JB007520, 2010.

Petrov, L. and Boy, J. P.: Study of the atmospheric pressure loading signal in very long baseline interferometry observations, Journal of Geophysical Research: Solid Earth, 109(B3), https://doi.org/10.1029/2003JB002500, 2004.

Qin, C., Zhong, S., and Wahr, J.: A perturbation method and its application: elastic tidal response of a laterally heterogeneous planet, Geophysical Journal International, 199(2), 631-647, https://doi.org/10.1093/gji/ggu279, 2014.

Ritsema, J., Deuss, A., Van Heijst, H. J., and Woodhouse, J. H.: S40RTS: a degree-40 shear-velocity model for the mantle from new Rayleigh wave dispersion, teleseismic traveltime and normal-mode splitting function measurements, Geophysical Journal International, 184(3), 1223-1236, https://doi.org/10.1111/j.1365-246X.2010.04884.x, 2011.

Rosat, S. and Hinderer, J.: Limits of detection of gravimetric signals on Earth, Scientific reports, 8(1), 1-8, https://doi.org/10.1038/s41598-018-33717-z, 2018.

Saito, M.: Excitation of free oscillations and surface waves by a point source in a vertically heterogeneous Earth, Journal of Geophysical Research, 72(14), 3689-3699, https://doi.org/10.1029/JZ072i014p03689, 1967.

Simmons, N. A., Forte, A. M., Boschi, L., and Grand, S. P.: GyPSuM: A joint tomographic model of mantle density and seismic wave speeds, Journal of Geophysical Research: Solid Earth, 115(B12), https://doi.org/10.1029/2010JB007631, 2010.

Sun, H., Zhang, H., Xu, J., Chen, X., Zhou, J., and Zhang, M.: Influences of the Tibetan plateau on tidal gravity detected by using SGs at Lhasa, Lijiang and Wuhan Stations in China, Terrestrial, Atmospheric and Oceanic Sciences, 30(1), 139-149, doi: 10.3319/TAO.2019.02.14.01, 2019.

Sun, W. and Okubo, S.: Surface potential and gravity changes due to internal dislocations in a spherical Earth—I. Theory for a point dislocation, Geophysical Journal International, 114(3), 569-592, https://doi.org/10.1111/j.1365-246X.1993.tb06988.x, 1993.

Takeuchi, H. and Saito, M.: Seismic surface waves, Methods in Computational Physics: Advances in Research and Applications, 11, 217-295, https://doi.org/10.1016/B978-0-12-460811-5.50010-6, 1972.

Tesoniero, A., Auer, L., Boschi, L., and Cammarano, F.: Hydration of marginal basins and compositional variations within the continental lithospheric mantle inferred from a new global model of shear and compressional velocity, Journal of Geophysical Research: Solid Earth, 120(11), 7789-7813, https://doi.org/10.1002/2015JB012026, 2015.

Trabant, C., Hutko, A. R., Bahavar, M., Karstens, R., Ahern, T., and Aster, R.: Data products at the IRIS DMC: Stepping stones for research and other applications, Seismological Research Letters, 83(5), 846-854, https://doi.org/10.1785/0220120032, 2012.

Tromp, J. and Trampert, J.: Effects of induced stress on seismic forward modelling and inversion, Geophysical Journal International, 213(2), 851-867, https://doi.org/10.1093/gji/ggy020, 2018.

Vermeersen, L. L. A. and Vlaar, N. J.: The gravito-elastodynamics of a pre-stressed elastic Earth, Geophysical Journal International, 104(3), 555-563, https://doi.org/10.1111/j.1365-246X.1991.tb05701.x, 1991.

https://doi.org/10.5194/egusphere-2022-661
Preprint. Discussion started: 3 August 2022
© Author(s) 2022. CC BY 4.0 License.

Van Camp, M. and Vauterin, P.: Tsoft: graphical and interactive software for the analysis of time series and Earth tides, Computers & Geosciences, 31(5), 631-640, https://doi.org/10.1016/j.cageo.2004.11.015, 2005.

Wahr, J. M.: Body tides on an elliptical, rotating, elastic and oceanless Earth, Geophysical Journal International, 64(3), 677-703, https://doi.org/10.1111/j.1365-246X.1981.tb02690.x, 1981.

Wahr, J. and Bergen, Z.: The effects of mantle anelasticity on nutations, Earth tides, and tidal variations in rotation rate, Geophysical Journal International, 87(2), 633-668, https://doi.org/10.1111/j.1365-246X.1986.tb06642.x, 1986.

Wang, H., Xiang, L., Jia, L., Jiang, L., Wang, Z., Hu, B., and Gao, P.: Load Love numbers and Green's functions for elastic Earth models PREM, iasp91, ak135, and modified models with refined crustal structure from Crust 2.0, Computers & Geosciences, 49, 190-199, https://doi.org/10.1016/j.cageo.2012.06.022, 2012.

Wang, R.: Tidal Deformations on a Rotating, Spherically Asymmetric, Viscoelastic and Laterally Heterogeneous Earth, (Doctoral dissertation), Retrieved from Peter Lang, Frankfurt am Main, 1991.

Wang, R.: Effect of rotation and ellipticity on Earth tides, Geophysical Journal International, 117(2), 562-565, https://doi.org/10.1111/j.1365-246X.1994.tb03953.x, 1994.

Wang, R.: Tidal response of the solid Earth, Tidal phenomena, 27-57, doi: 10.1007/BFb0011456, 1997.

Wang, X., Holt, W. E., and Ghosh, A.: Joint modeling of lithosphere and mantle dynamics: Evaluation of constraints from global tomography models, Journal of Geophysical Research: Solid Earth, 120(12), 8633-8655, https://doi.org/10.1002/2015JB012188, 2015.

Yuan, L., Chao, B. F., Ding, X., and Zhong, P.: The tidal displacement field at Earth's surface determined using global GPS observations, Journal of Geophysical Research: Solid Earth, 118(5), 2618-2632, http://doi.org/10.1002/jgrb.50159, 2013.

Zhao, D.: Seismic structure and origin of hotspots and mantle plumes, Earth and Planetary Science Letters, 192(3), 251-265, https://doi.org/10.1016/S0012-821X(01)00465-4, 2001.

https://doi.org/10.5194/egusphere-2022-661
Preprint. Discussion started: 3 August 2022
© Author(s) 2022. CC BY 4.0 License.

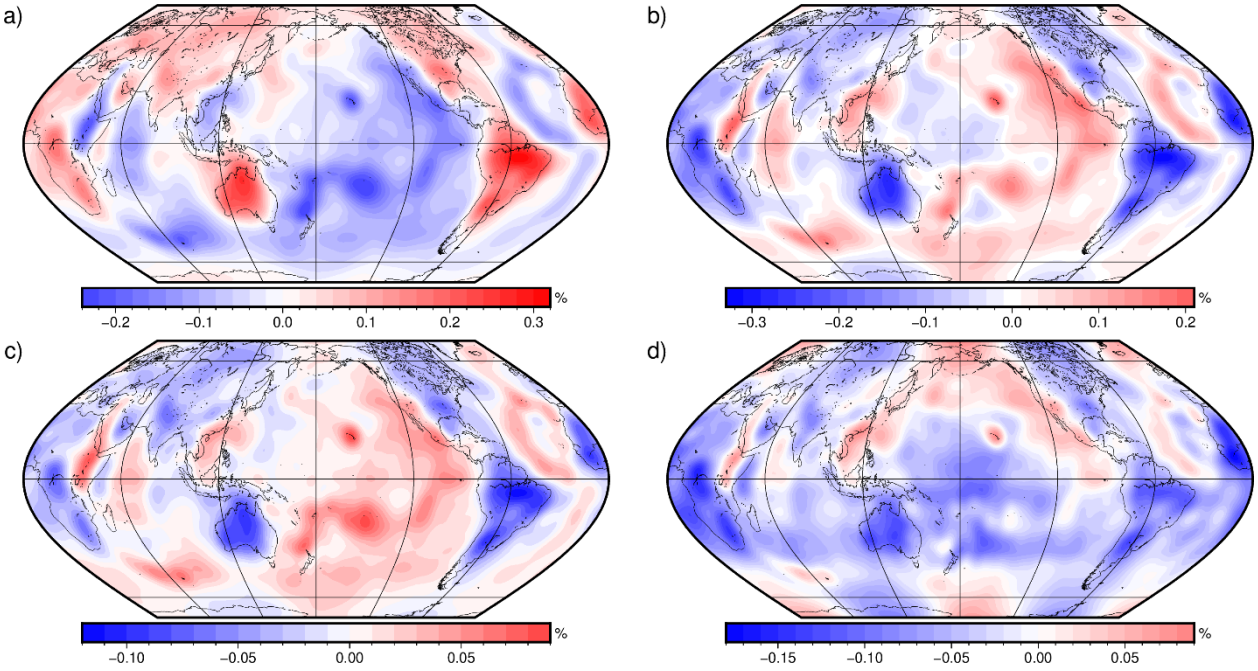

Figure 1: Changes in the semidiurnal gravimetric factor resulting from a) the P-wave velocity disturbance, b) the S-wave velocity disturbance, c) density disturbance, and d) total changes, i.e., identical to the summation of a), b), and c). Results illustrated in a) are calculated by the GyPSuM P-wave model and in b) are calculated by the GyPSuM S-wave model. Results in c) are calculated by the GyPSuM density model, gravity model and its derivative. The influences of the density model are much larger than those of gravity model and its deriavative, and as a result, it can be stated for convenience that the changes result from density disturbance. Results in d) are changes as calculated by the three-dimensional Earth model GyPSuM respective to the spherically-symmetrical Earth model PREM (Dziewonski and Anderson, 1981).

https://doi.org/10.5194/egusphere-2022-661
Preprint. Discussion started: 3 August 2022
© Author(s) 2022. CC BY 4.0 License.

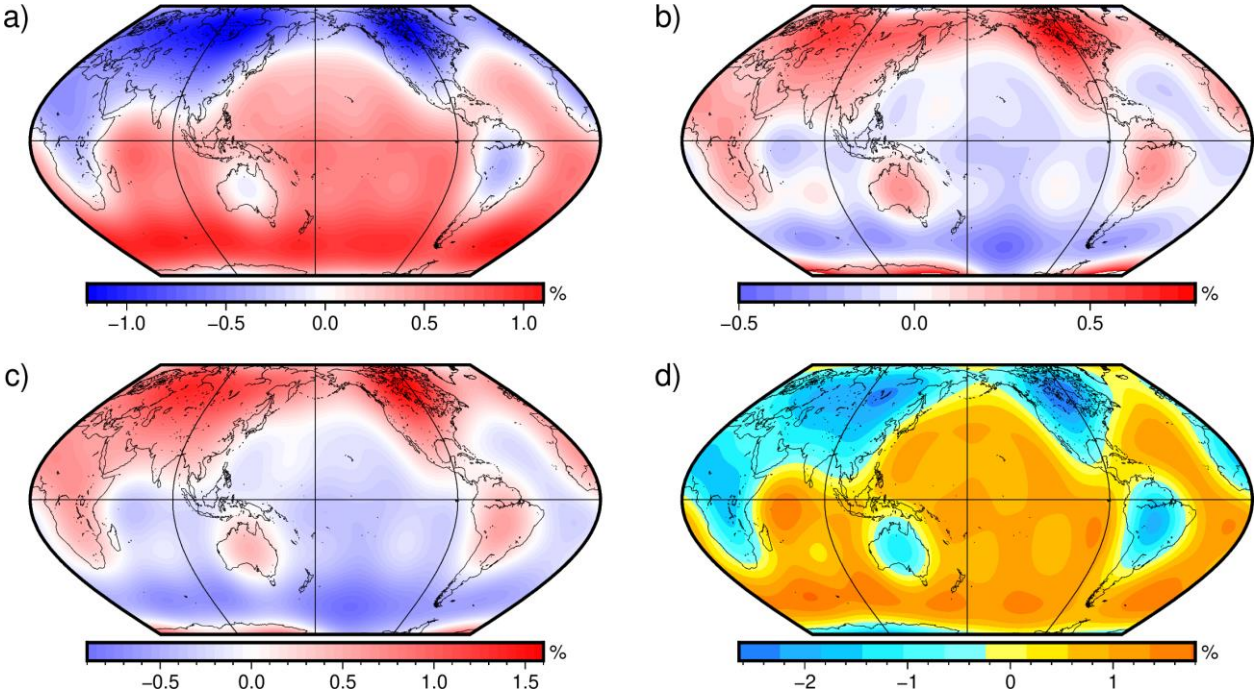

Figure 2: Changes in semidiurnal gravimetric factors calculated for the ocean-land model. Effects of a) the P-wave velocity disturbance, b) the S-wave velocity disturbance, c) the density disturbance, and d) the input ocean-land model are illustrated. All patterns of the a), b), and c) are consistent with the ocean-land model d) to some extent. The value under the ocean is generally positive whereas the value under the continent is generally negative in a), and vice versa in b) and c). The three kinds of effects are almost at the same level.

https://doi.org/10.5194/egusphere-2022-661
Preprint. Discussion started: 3 August 2022
© Author(s) 2022. CC BY 4.0 License.

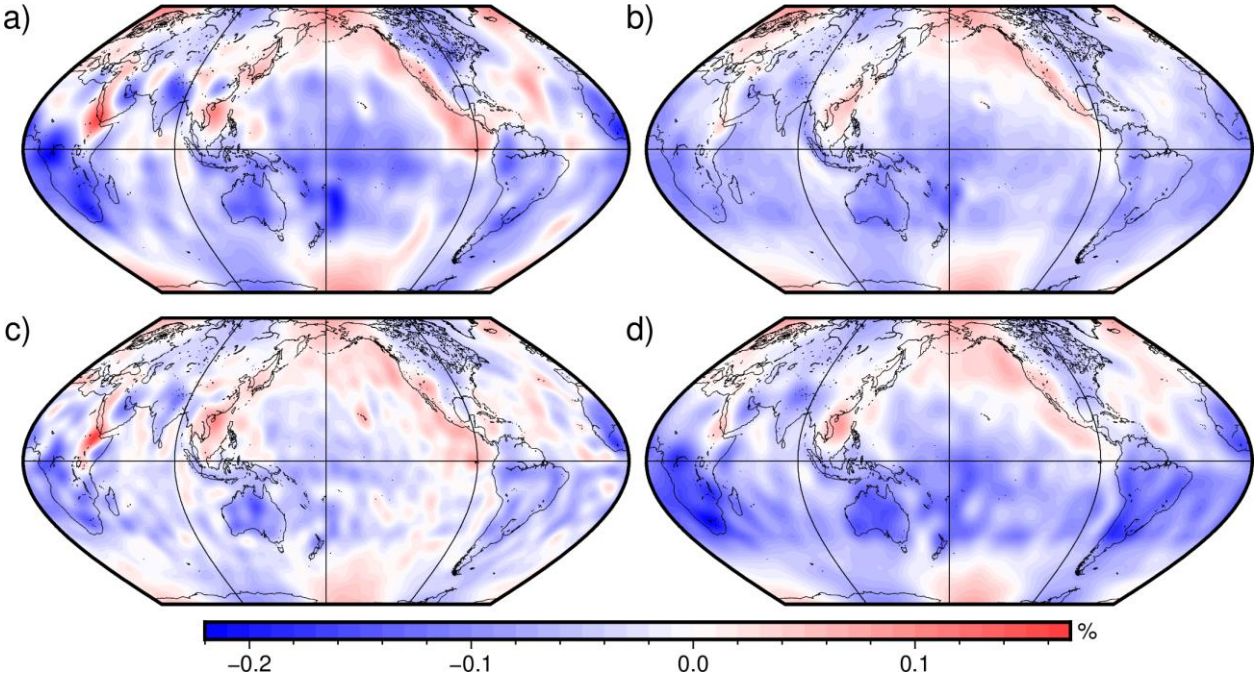

Figure 3: Total changes in the semidiurnal gravimetric factors calculated by the three-dimensional Earth models. a) SPani, b) SEISGLOB2, c) SGLOBE-rani, and d) SAW64ANb.

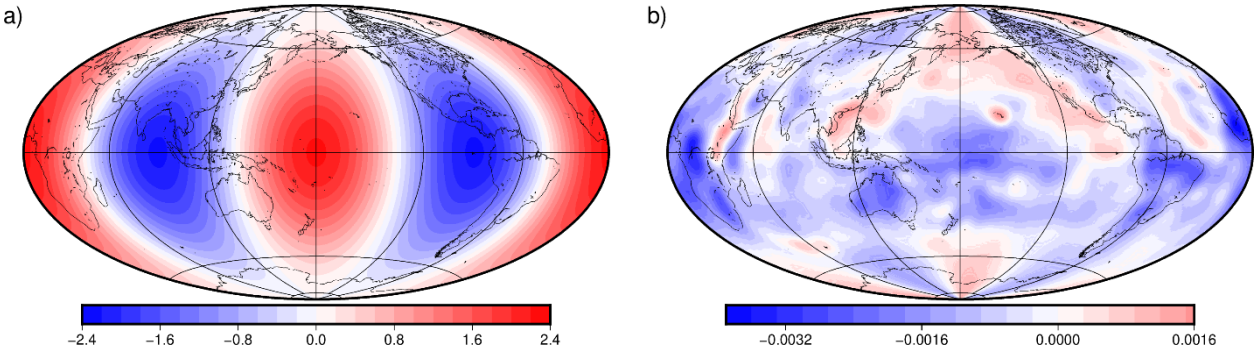

Figure 4: Gravity changes for a) $\Delta g_0(\theta, \phi, t = 0)$ resulted from semi-diurnal tide-generating potential and b) $\Delta g_{3-D}(\theta, \phi)$ resulted from laterally-inhomogeneous disturbance. The three-dimensional Earth model GyPSuM is used for calculating $\Delta g_{3-D}(\theta, \phi)$.

https://doi.org/10.5194/egusphere-2022-661
Preprint. Discussion started: 3 August 2022
© Author(s) 2022. CC BY 4.0 License.

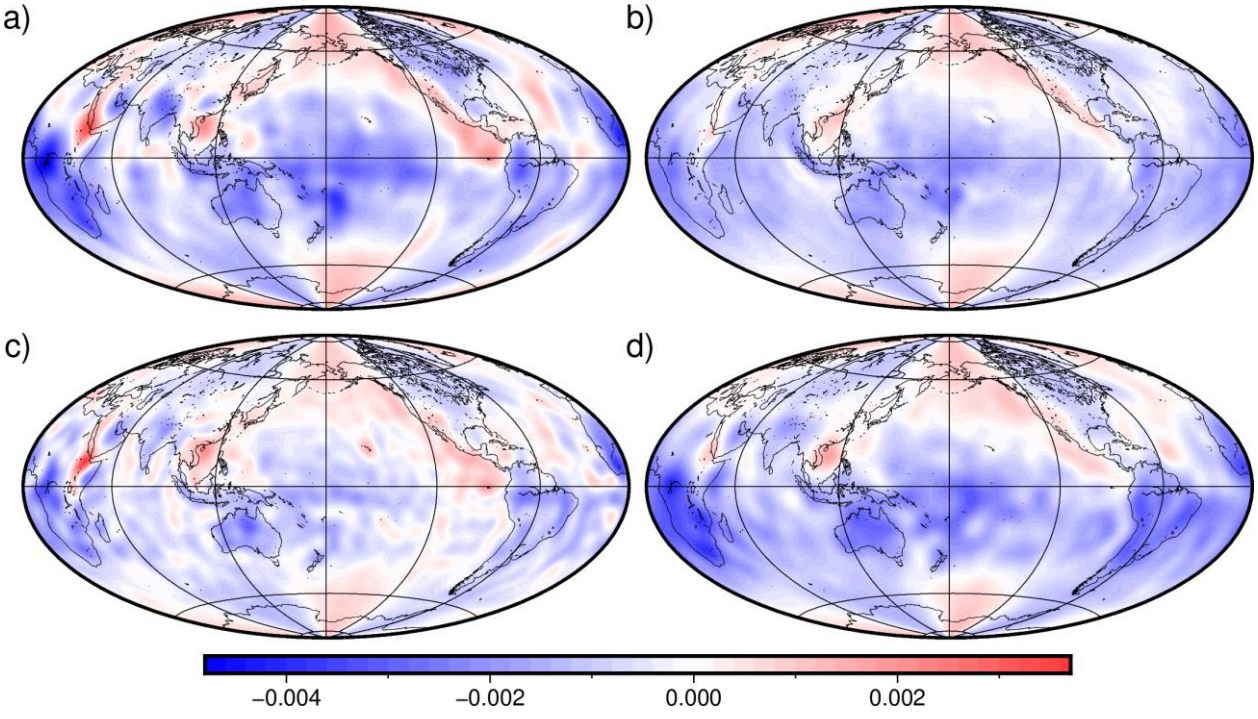

Figure 5: Changes in the semidiurnal tidal gravity calculated by the three-dimensional Earth models. a) SPani, b) SEISGLOB2, c) SGLOBE-rani, and d) SAW64ANb.

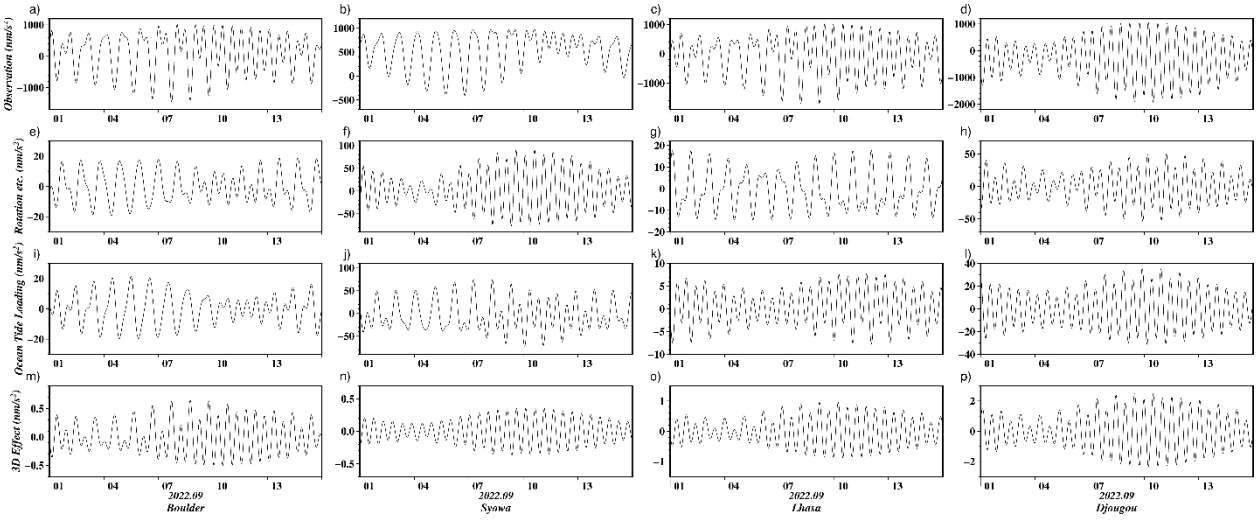

Figure 6: Prediction of tidal gravity variations in Boulder (the first column), Syowa (the second column), Lhasa (the third column), and Djougou (the fourth column). The first row shows the total tidal signal calculated by the observed gravimetric factors. The second row shows the effects of rotation, ellipticity, inelasticity, and non-hydrostatic structure. The third row shows the ocean tide loading effect. The fourth row shows the lateral inhomogeneity effect.

https://doi.org/10.5194/egusphere-2022-661
Preprint. Discussion started: 3 August 2022
© Author(s) 2022. CC BY 4.0 License.

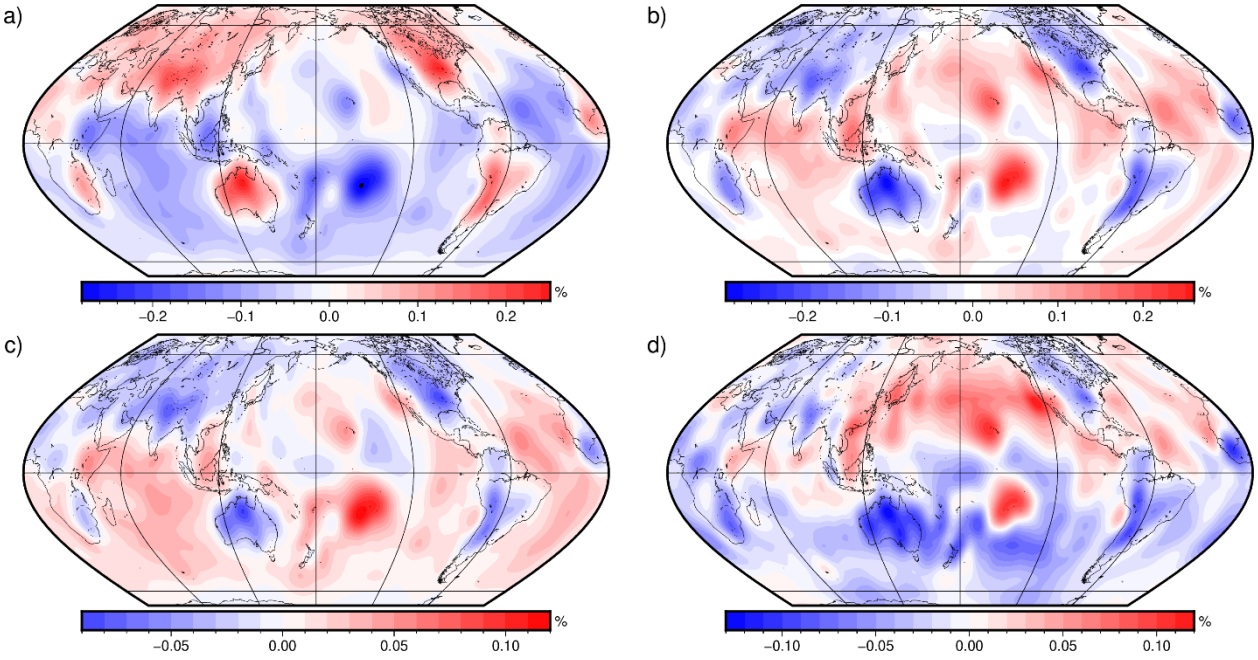

Figure F1: Same as Figure 1 but calculated by Zhao's (2001) three-dimensional Earth model.

765 **Table 1: Information for superconducting gravimeters and M2 factors**

Location	Latitude (°)	Longitude (°)	Altitude (m)	δ_m	$\Delta\delta_e$	$\Delta\delta_{3D}$
Boulder	40.131	254.767	1682	1.15944±0.00010	0.0039	-0.00025
Cantley	45.585	284.193	269	1.20349±0.00005	0.0039	-0.00063
Canberra	-35.321	149.008	762	1.18585±0.00004	0.0038	-0.00049
Esashi	39.151	141.332	434	1.19300±0.00009	0.0039	0.00025
Matsushiro	36.544	138.203	451	1.19098±0.00007	0.0038	0.00022
Syowa	-69.007	39.595	24	1.40054±0.00051	0.0041	0.00134
Wuhan	30.516	114.490	89	1.17159±0.00006	0.0038	0.00000
Membach	50.609	6.007	250	1.18824±0.00012	0.0040	0.00014
Metsahovi	60.217	24.396	56	1.18187±0.00022	0.0041	0.00012

https://doi.org/10.5194/egusphere-2022-661
Preprint. Discussion started: 3 August 2022
© Author(s) 2022. CC BY 4.0 License.

Potsdam	52.381	13.068	81	1.18585±0.00004	0.0040	0.00057
Strasbourg	48.622	7.684	180	1.18710±0.00008	0.0040	-0.00042
Vienna	48.249	16.358	80	1.18170±0.00003	0.0039	-0.00013
Lhasa	29.645	91.035	3632	1.16289±0.00002	0.0038	-0.00026
Lijiang	26.896	100.232	2435	1.16575±0.00004	0.0037	-0.00023
Djougou	9.842	1.606	483	1.17265±0.00002	0.0036	-0.00127